DESIGN AND NUMERICAL ANALYSES OF GUIDE VANES OF A MULTISTAGE SUBMERSIBLE PUMP

A Thesis Submitted to
The Graduate School of Engineering and Science of
İzmir Institute of Technology
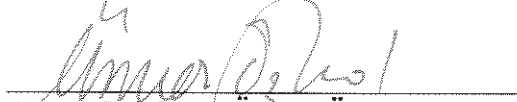in Partial Fulfillment of the Requirements for the Degree of

MASTER OF SCIENCE

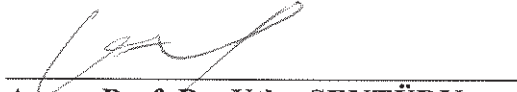in Mechanical Engineering

by
Mert DEMİRTAŞ

July 2019
İZMİR

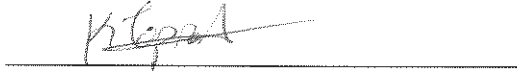We approve the thesis of **Mert DEMİRTAŞ**

Examining Committee Members:

_____
Assoc. Prof. Dr. Ünver ÖZKOL
Department of Mechanical Engineering, İzmir Institute of Technology

_____
Assoc. Prof. Dr. Utku ŞENTÜRK
Department of Mechanical Engineering, Ege University

_____
Assist. Prof. Dr. Kasım TOPRAK
Department of Mechanical Engineering, İzmir Institute of Technology

12 July 2019

_____
Assoc. Prof. Dr. Ünver ÖZKOL
Supervisor, Department of Mechanical
Engineering, İzmir Institute of
Technology

_____
Prof. Dr. Sedat AKKURT
Head of the Department of Mechanical
Engineering

_____
Prof. Dr. Aysun SOFUOĞLU
Dean of the Graduate School of
Engineering and Sciences

ACKNOWLEDGMENTS

ABSTRACT

DESIGN AND NUMERICAL ANALYSES OF GUIDE VANES OF A MULTISTAGE SUBMERSIBLE PUMP

The objective of this thesis is to analyze a multistage submersible pump numerically, figure out the inefficient sections of flow and propose a modified design according to the simulation results.

Hydraulic parts of a submersible pump are impeller, diffuser and return channel. In this study, the investigated pump's stages have only impellers and return channels. According to the literature, the inefficiencies in pump stages might be caused by angle misalignment of impeller and guide vanes, channel geometries or vane designs.

The investigated five stage submersible pump and its CAD models are provided by a manufacturing company. In the first part of the study, fluid domain is created for numerical computations and analyses are performed with ANSYS Fluent software. According to the simulation results, flow nonuniformities are observed in return channels and identified that the reason is guide vane geometry. The second part of the study includes the modified design of guide vane and set of simulations with different wrap angles to find out the optimized value.

The simulation results of this thesis study are quite satisfactory when they are compared to experimental data of manufacturing company. After modifications, the nonuniformities which are observed in original design are diminished and efficiency of the pump is increased.

ÖZET

KADEMELİ BİR DALGIÇ POMPANIN KILAVUZ KANATLARININ DİZAYNI VE NÜMERİK ANALİZLERİ

Bu tezin amacı, kademeli bir dalgıç pompayı nümerik olarak analiz etmek, akışın verimsiz bölümlerini bulmak ve simülasyon sonuçlarına göre yeni bir tasarım önermektir.

Bir dalgıç pompanın hidrolik parçaları, çark, difüzör ve dönüş kanalıdır. Bu çalışmada, incelenen pompanın kademelerini yalnızca çarklar ve geri dönüş kanalları oluşturmaktadır. Literatüre göre, pompa kademelerindeki verimsizlikler, çark ve kılavuz kanatlarının açı hizalamalarındaki uyumsuzluktan, kanal geometrilerinden veya kanat tasarımlarından kaynaklanabilir.

İncelenen beş kademeli dalgıç pompa ve CAD modelleri bir üretici tarafından sağlanmıştır. Çalışmanın ilk bölümünde, nümerik hesaplamalar için akışkan alanı oluşturulmuştur ve analizler ANSYS Fluent programı kullanılarak gerçekleştirilmiştir. Simülasyon sonuçlarına göre geri dönüş kanallarında akış düzensizlikleri gözlenmiştir ve sebebin kılavuz kanat geometrisi olduğu tespit edilmiştir. Çalışmanın ikinci bölümü, yeni kılavuz kanadının tasarımını ve optimize edilmiş değeri bulmak için farklı tarama açıları ile yapılmış olan simülasyon kümesini içerir.

Bu tez çalışmasının simülasyon sonuçları, üretici firmanın deneysel verileri ile karşılaştırıldığında oldukça tatmin edicidir. Değişikliklerden sonra, orijinal tasarımda gözlenen düzensizlikler azalmıştır ve pompanın verimi arttırılmıştır.

TABLE OF CONTENTS

LIST OF FIGURES

x

LIST OF TABLES

LIST OF SYMBOLS

SYMBOLS

a_1	closure constant (see Eq. 2.8)
b	return channel width at L-bend
b_c	return channel width at crossover bend
b_1	impeller channel width at inlet
b_2	impeller channel width at exit
h	loss
$\dot{m}$	mass flow rate
n	rotational speed
u	circumferential velocity
v	absolute velocity
w	relative velocity
z	impeller blade number
D_1	impeller eye diameter
D_2	impeller diameter
D_w	cross-diffusion term
F_1	blending function
G	turbulence generation
H	actual head
H_i	ideal head
K_1	coefficient (see Eq. 1.2)
K_2	coefficient (see Eq. 1.3)
K_6	coefficient (see Eq. 1.4)
N	specific speed
P_{t2}	total pressure at return channel inlet
P_{t3}	total pressure at return channel outlet
P_{s2}	static pressure at return channel inlet
Q	capacity
Q_s	shockless capacity
R	mean streamline curvature radius

Y	turbulence dissipation	
α	flow angle	
β	impeller blade angle	
θ	wrap angle	
ϕ	guide vane angle	
η	efficiency	
ρ	density	
σ	slip factor	
τ	shear stress	
μ	absolute viscosity	
ξ	loss coefficient	
Γ	effective diffusivity	

INDICES

1	inlet of the blade
2	exit of the blade
d	diffusion
f	friction
k	turbulence kinetic energy
w	specific dissipation rate
r	radial
t	tangential

CHAPTER 1

INTRODUCTION

According to *Dictionary of Mechanical Engineering* (Atkins and Escudier 2013). A pump is "a machine designed to cause a liquid, gas, vapour, or slurry to flow due to the reciprocating motion of pistons, rotation of vanes, or rotation of impeller". The terminology includes all variations of pumps. However, this study focuses on performance of an electrical submersible pump (ESP) which is a multistage centrifugal pump type working at fluid level and in vertical position.

The aim of this thesis is the performance evaluation, finding out and reducing the inefficiencies of a particular submersible pump. As a beginning, the history of ESPs, operational features, pump hydraulics and numerical analysis techniques for rotating machines are briefly presented. In following sections, geometric modifications on the model, their reasons and results are explained.

1.1. History of Pumps

Application of fluid lifting begins with the invention of the shadoof by Egyptians in 2000 BC. Shadoof, is a hand-operated tool based on moment of force concept. Then, ancient civilizations use waterwheel for irrigation. In 200 BC, screw pump is found by Archimedes and its developed versions are still in use (Yannopoulos, et al. 2015).

After 17th century, an unstoppable mechanical development chain is occured and pumps develop with the invention of steam engine. There is not a certain information about discovery of the centrifugal pumps, but many sources accept Denis Papin, a French inventor, for the founder of centrifugal pump (Robinson 1947). Papin's pump creates vortex by means of straight vanes. Then, in 1838, the importance of the curvature at the impeller vanes come to light with a publication of Combs. In following years, British inventor, John Appold's experiments show that the efficiency of the centrifugal pump depends on the blade curvature (Girdhar and Moniz 2004). In addition to this, the first multistage centrifugal pump is constructed in same years.

<center>(a)   (b)</center>

Figure 1.1 History of pumps (a) Shadoof by Egyptians (Source: Yannopoulos, et al. 2015), (b) Archimedes screw pump (Source: Britannica 2014).

Electrical Submersible Pumps, ESP are started to be used in early 1900s. ESPs are the remarkable machines in industrially growing world and highly satisfying for high-volume needs of oil and water. In 1916, a Russian company owner, Armais Arutunoff, designed a centrifugal pump attached to an electrical motor for drainage applications. After a decade, this design is developed and possesses a small diameter with multiple stages. In 1926, the first ESP is installed for an oil well in Kansas by Arutunoff's company (ESPpump.com n.d.).
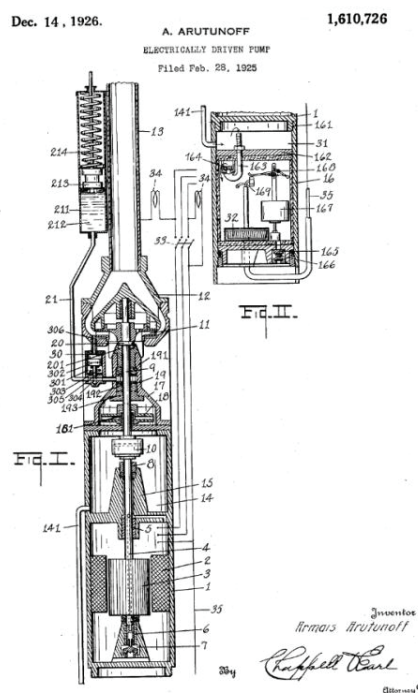
Figure 1.2 Arutunoff's ESP (Source: Arutunoff 1926)

1.2. Types of Pumps

Pumps are classified according to their operation principle, flow direction, geometry or type of design. The simple classification is to divide the pumps on the basis of their working principle.
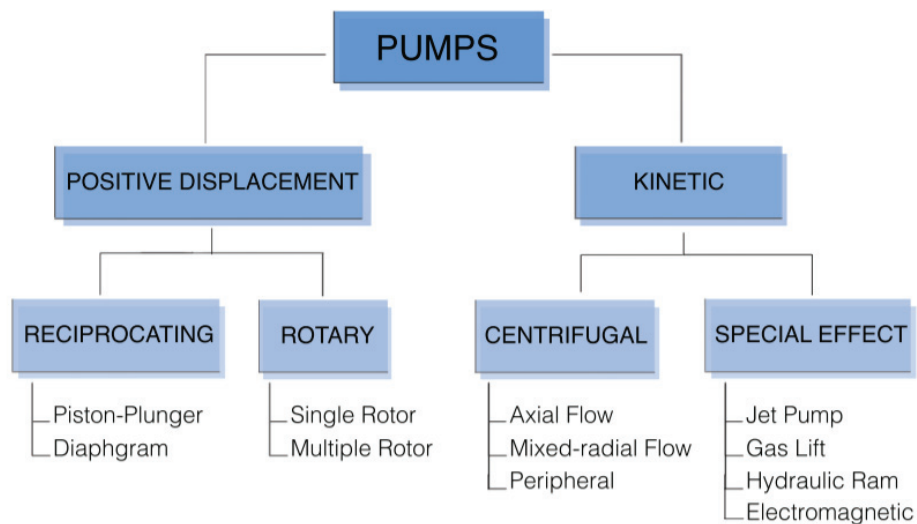
Figure 1.3 Diagram of pump classification

A positive displacement pump, takes the fluid from suction side to fixed volumes and forces it to the discharge by increasing the pressure. Displacement pumps are highly efficient and have better handling for viscous fluids than dynamic pumps, however they are not capable of working at high velocities due to the threat of erosion. Besides, when displacement pumps are operated, the energy is added periodically and this creates stuttering which is not desirable. Unlike displacement pumps, kinetic pumps generate head by increasing the fluid velocity which is gained from rotation. Kinetic energy is continuously added and converted to hydrodynamic energy, since the efficiency is lower than displacement pumps due to the conversion. Kinetic pumps can operate at higher velocities and have less installation and maintenance cost relative to the others. Additionally, they have one rotating shaft which makes the phenomenon very simple. Therefore, kinetic pumps are the most common machines in hydraulic applications.

Apart from these categories, there are special effect such as jet pump, gas lift pump, hydraulic ram and electromagnetic pump. They serve for particular applications and all have specific operating principles.

Centrifugal pumps are classified according to the flow direction in itself. The reason of this classification is a characteristic called specific speed which is introduced by Camerer for water turbines and pumps in 1914. It gives foreknowledge to designer about the vane shape and efficiency in accordance with the design conditions. In low specific speeds, radial vanes can handle the flow efficiently. However, vane shape changes from radial to axial in high specific speeds in order to preserve the efficient flow (Figure 1.4).Specific speed is defined as,

$$N_s = \frac{n\sqrt{Q}}{H^{3/4}} \tag{1.1}$$

where; n is revolution per minute, Q is gallons per minute and H is feet. Specific speed can be calculated in metric system as well by using cubic meter per hour for Q and meters for H. Karassik and Wislicenus specified the relation between U.S. and metric systems as $N_s = 51.65 N_{Sm}$. (Karassik, et al. 1986).

Specific speed is a dimensionless number. It does not change for a particular pump and it is same at all angular velocities. In multistage pumps, specific speed is calculated for the first stage.
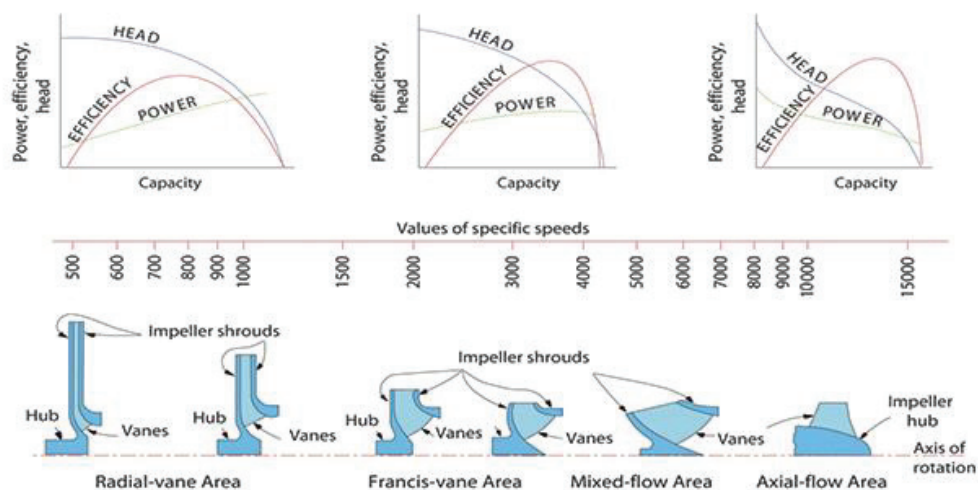
Figure 1.4 Vane profiles for different specific speed values in U.S. system. (Source: Chaurette 2003)

1.3. Electrical Submersible Pump and Major Components

ESP's are the most efficient and very commonly used device for fluid lifting applications. They take place in many fields, such as oil and water extraction, drainage systems or water supply for residents and industrial areas.

<center>(a)   (b)</center>
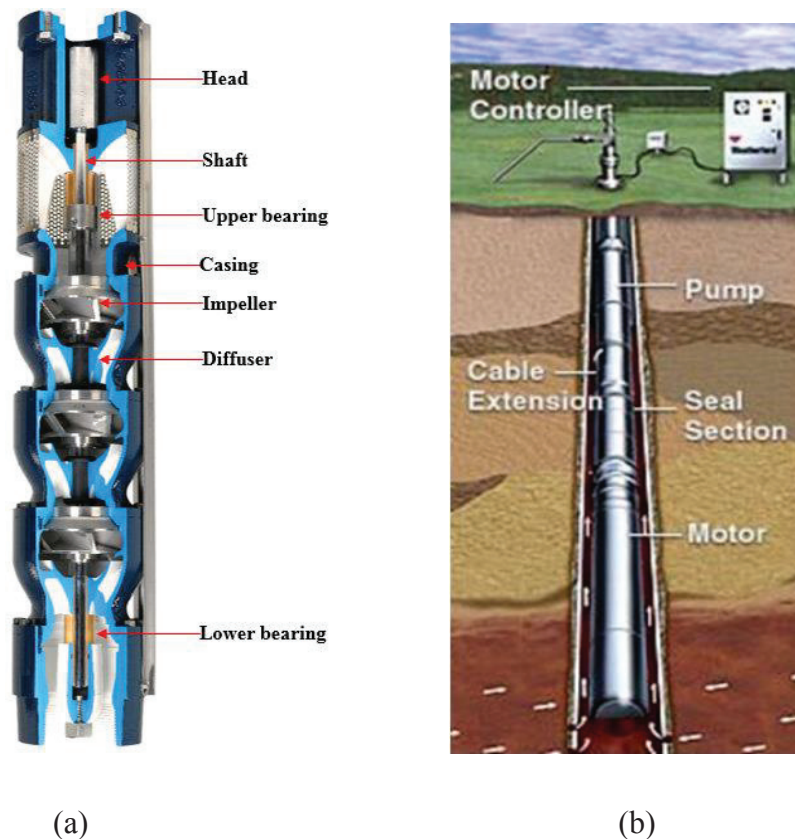
Figure1.5 ESP system (a) Section view of a multistage submersible pump (Source: Zhu and Zhang 2018), (b) Settling of ESP components in pumping system (Source: New Mexico Tech 2015)

There are some key features that make ESP systems highly favorable (Hollund 2010).

- They have a compact design and provide easy installation.
- They can operate in narrow wells due to the vertical assembled setup.
- They are not affected from high fluid temperatures, also they have a wide capacity and head range.

- Cavitation which is a crucial fact for the pumps out of water, is not a problem, since they are submerged in fluid.

Considering these features, submersible pumps are different from jet pumps, despite both do the same job. Submersible pumps are located in wells and push the fluid from the operating level, as jet pumps work at ground level and lift the fluid by sucking.

ESP systems are made up from several main components. The heart of an ESP is a multistage centrifugal pump, containing an impeller and a diffuser or guide vanes connected to the casing for each stage. Electric motor and sealing components help the pump to provide a smooth operation.

1.3.1. Impeller

Impeller is the rotating part of a centrifugal pump. It may include different number of vanes attached to the hub. Impeller is connected to the electric motor with a shaft and it does the main objective which is converting the rotational kinetic energy to pressure.

As mentioned in the previous chapter, impellers are classified according to the flow path of the fluid. Also, they can be divided into three by the basis of mechanical designs. Open, semiopen and closed impeller designs which are indicated in Figure 1.6 are used for different applications. Open impellers look like propellers, they consist of curved vanes attached to a hub. Semiopen impellers involve a single back shroud and mounted vanes. Closed design is the most used type in impeller variations. It is enclosed by two shrouds at the back and front, so it allows the fluid to move between sidewalls of the vanes.

Both open and closed impeller are highly used in industry. However, closed type impellers are preferred for submersible systems, since the working fluid might be explosive in oil industries and closed impellers prevent any possible sparks to reach the fluid. Besides, despite open type impellers are simpler, closed type impellers guide the fluid better and have much smaller clearances as opposed to the open types. Therefore, waste of energy is prevented (Mc Nally Institute 2018).
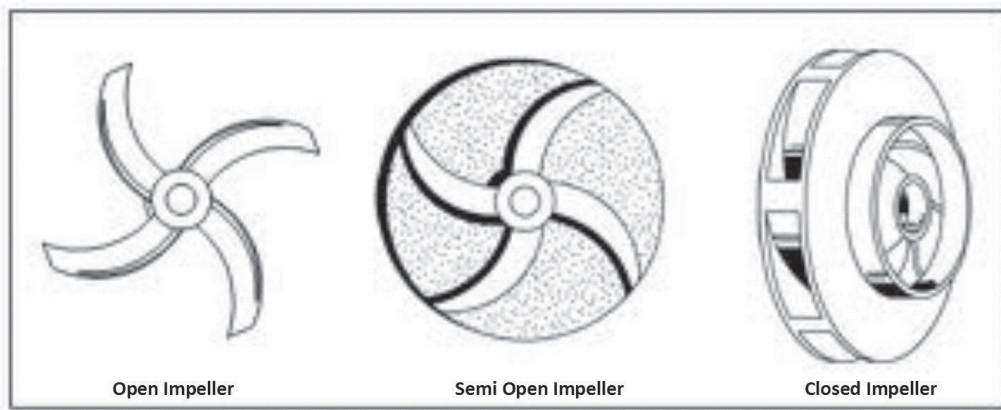
Figure 1.6 Impellers with different shroud variations (Source: Jones and Vanderholm n.d.)

Another parameter which is used in impeller design is blade curve shape. Blades differ according to blade exit angle β_2. It is clear in Figure 1.7 that forward curved blades have an exit angle above 90°, backward curved blades have below 90° and radial blades are perpendicular to the rotational axis.
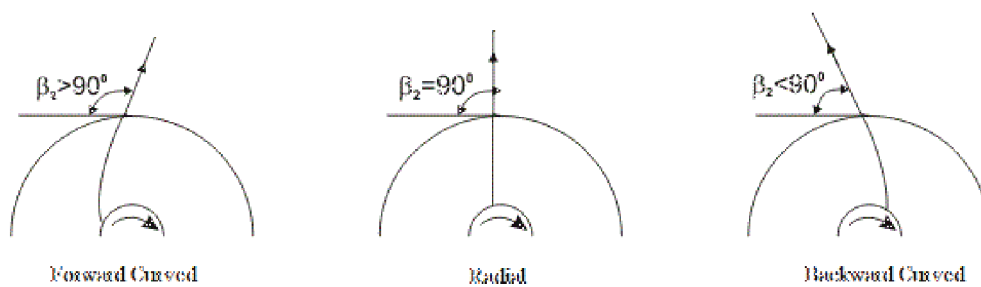
Figure 1.7. Impeller types according to vane angles (Source: Nptel n.d.)
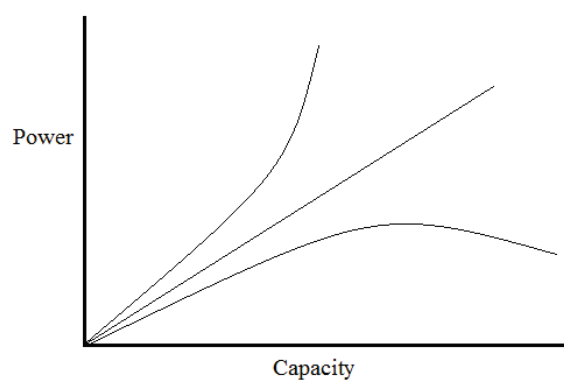
Figure 1.8 Power-capacity curves according to vane angles (Source: Nptel n.d.)

In centrifugal pumps, backward curved bladed impellers are preferred mostly. The reason is that the backward curved blades provide more efficient flow than the other shapes (Oyelami, et al. 2012). Besides, the power curves in Figure 1.8 show that backward curved designs have a maximum power value which acts as a self control, while power increases continuously in forward curved designs that may cause motor overloads at high flow rates.

Different types of impellers are shown in Figure 1.9 and they are the most efficient types in their own application areas.

(a)   (b)   (c)
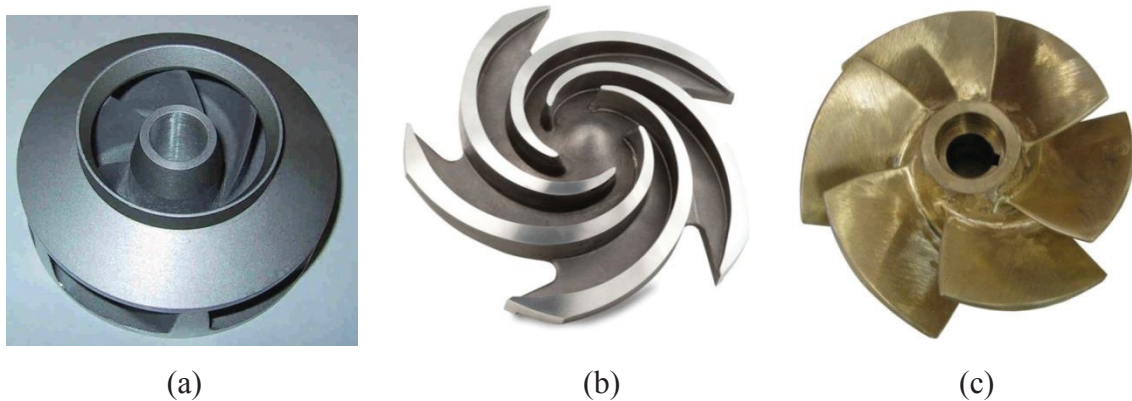
Figure 1.9 Different type of impellers (a) Closed Impeller (Source: Indiamart n.d.), (b) Open impeller (Source: Elsey 2017), (c) Mixed flow impeller (Hydra-Tech 2016).

1.3.2. Diffuser

In one stage of a centrifugal pump, impeller and diffuser work with in cooperation. While the impeller accelerates the fluid and creates head, task of a diffuser is to convert the leftover tangential kinetic energy to pressure and to minimize the expected losses. Diffusers have two main principles to recover the kinetic energy loss;

- They decrease the average velocity by extending the flow area, this results as a static pressure rise.
- They change the radius of the flow passage and create angular momentum recovery in radial diffusers (Japikse, Marscher and Furst 1997).

Diffusers can be mounted to periphery of the impeller (Figure 1.10a) or they can be assembled as a stage component (Figure 1.10b).

<div align="center">(a)   (b)</div>
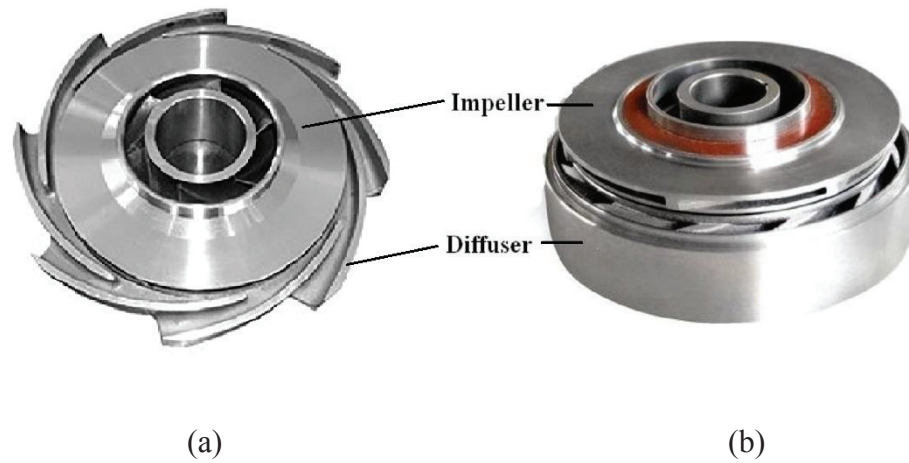
Figure 1.10 Impeller-diffuser fittings (a) Diffuser mounted to impeller periphery (Source: Indiamart n.d.), (b) Diffuser as a stage element (Source: Abbas, Asker and Ali 2012).

1.3.3. Return Channel and Guide Vanes

Unlike diffusers, return channels does not increase pressure by enlarging the flow area. The job of return channel vanes is to remove and recover the swirl by transforming the tangential kinetic energy to static pressure (Lee, et al. 2016). Return channels are always attached to an impeller and they are distinct stage elements. As seen in Figure 1.11, return channel is located at the end of a stage. The reason of this alignment is that, return channels and guide vanes recover the losses and regulate the flow which enters to impeller of next stage or outlet pipe where, rotational flow creates frictional loss.

In literature, there is not an accurate design for return channel blades because of the flow profile which is different for each impeller. However, Akaike and Toyokura's experiments show that the flow exits from U-turn type return channel uniformly. Their suggestion is to design return channel blades two dimensionally which means without distortion and twist (Akaike and Toyokura 1979). The radial layout of blades is important to avoid tangential velocity occurance before the fluid enters the impeller of next stage. Roclawski, replaced a three dimensional stator with two dimensional

diffuser like vanes and gained 28% increase in hydraulic head (Roclawski, Weiten and Hellmann 2006).

Cheah showed in his study that the flow separation occurs at the inner surface of the passage for a curved flow because of the free vortex flow.
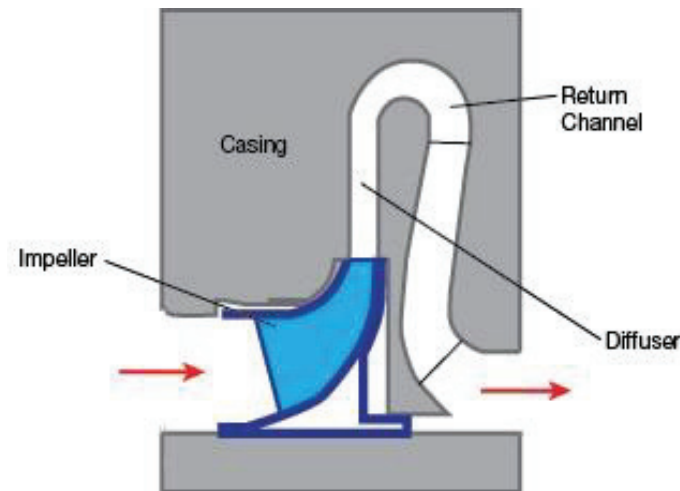
Figure1.11 Meridional view of a single stage of turbomachinery (Source: Harvey 2017)

Besides, possible design suggestions are made for flow passage of return channels. The most accepted one is Aungier's parameter of channel width and U-bend curvature, which is explained and implemented in Chapter 4 (Hildebrandt, Aerodynamic optimisation of a centrifugal compressor return channel and U-turn with genetic algorithms 2011).

1.3.4. Electric Motor

Electric motor is the energy source of the system, it provides the necessary mechanical energy to the pump shaft which rotates the impellers in stages. Motors in ESP systems are usually three-phase, two pole, squirrel cage induction type motors. These motors are cheap, robust and the most efficient type for deep well applications. However there are some handicaps due to the operating conditions (Takacs 2009).

- Increasing the power is achieved only by increasing the length of the motor because of the limited radius.

- A perfect sealing system is inevitable.
- Considerable voltage drops are encountered due to the long cable connections between motor and the electric source on the ground.
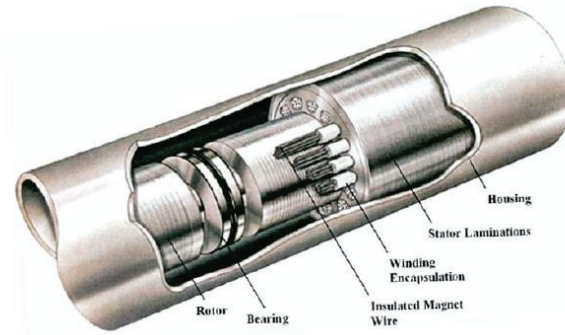
Figure 1.12 Submersible pump motor (Source: Hollund 2010).

1.3.5. Sealing

ESP systems consist of a protector section to prevent the operating fluid to fill into the electrical motor and cause low-circuit or burning. It is placed between the motor and the intake part. Protector provides the equalization of the pressure in the motor in order to avoid rapid expansions due to the high temperatures. Additionally, this section acts as a housing for the shaft going out from the motor (Takacs 2009). Apart from the protector, primary rings and mating rings are the most common components for a mechanical sealing. Primary rings which generally move with the shaft, are the flexible pieces for rotating processes. Mating rings are used between stationary components or gland plate of the pump. The only task of these components is to eliminate any leakage in the pumping system.
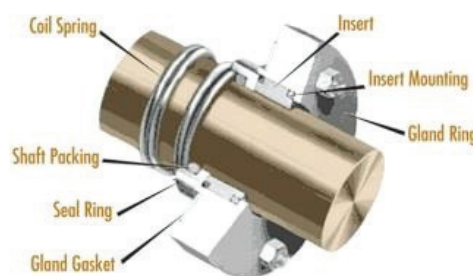
Figure 1.13 Rings fitted on shaft to prevent leakage (Source:Japikse, Marscher and Furst 1997)

1.4. Flow Inefficiencies and Losses in Pumps

In engineering nomenclature, efficiency is the ratio between the amount of energy produced and the amount of energy used (Collin 1984). For pumps it is the relation between the power delivered to water from pump and the shaft power input. Efficiency concept arise from the energy losses which occur in different parts of a pump. These main sources of inefficiency can be classified as mechanical losses, volume losses and hydraulic losses.

Mechanical losses include disk friction loss, stuffing box loss and bearing losses. Big portion of mechanical inefficiency is caused by disk friction loss which is created by the fluid flow between the rotating impeller and the stationary casing walls. Squeezed fluid particles start moving and creates centrifugal forces which do notable effects in pump efficiency when operating especially at low specific speeds. Studies and experiments point out that disk friction losses can be decreased by minimizing the gap between the walls (Feng, et al. 2017). Mechanical friction losses may cover 3-4% of total efficiency.

Volume losses are the capacity losses through clearances between pump parts. Leakages through flow passages, impeller eye, impeller neck, wearing rings or between the stages in multistage pumps may lead to reduction of pump volumetric efficiency. Zhao's studies about the wearing ring clearance effects (Zhao, et al. 2012) and Wood's experiments about tip clearance effects on pump performance (Wood, Welna and Lamers 1965) indicate that, leakage losses affect the pump performance around 2% which is a small value compared to other types of inefficiencies.

Even though mechanical and volume losses do remarkable effects on pump performance, hydraulic losses have a big share in most of the total inefficiency. Hydraulic losses are caused by skin friction, diffusion, flow separation, shocks at rotor inlets and mixing losses at discharges. Friction loss is the energy decrement due to skin the friction between the moving fluid and the enclosing surface.

A coefficient K_1 is accepted to express the all frictional effects and lengths for a specific pump and the loss is formulated as;

$$h_f = K_1 Q^2 \qquad (1.2)$$

where, h_f is the loss due to the friction and Q is the capacity. A similar expression is also given for the diffusion losses as well.

$$h_d = K_2 Q^2 \qquad (1.3)$$

Fluid flow at the entrance or exit regions of the impeller and diffuser is shocked due to the sudden changes in velocity magnitude and direction. Besides, flow tends to separate when encountered to sharp turns at pump vanes or volute. Eddies and wake mixing occur at the discharge of the impeller because of the shear between the high velocity, swirling outflow and the more uniform fluid in volute. A general expression for shock losses is determined by means of capacity;

$$h_s = K_6 (Q - Q_s)^2 \qquad (1.4)$$

where, Q is capacity, Q_s is shockless capacity and K_6 is a constant for a given pump. Derivation of the losses and the constants are explained in details by Stepanoff (Stepanoff 1957).
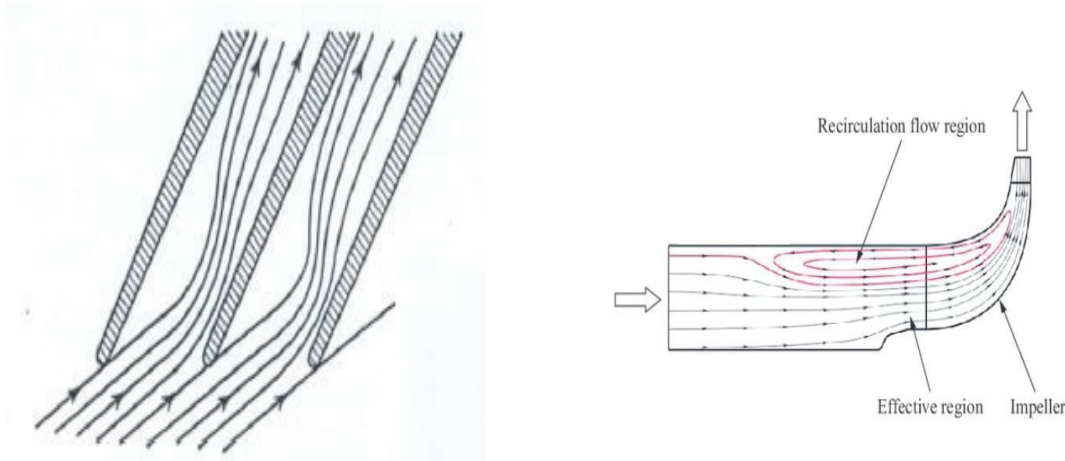
Figure 1.14 Examples of hydraulic losses (a) Enterance shock loss (Source: Stepanoff 1957), (b) Recirculation due to sharp turn (Source: Tamaki, et al. 2016)
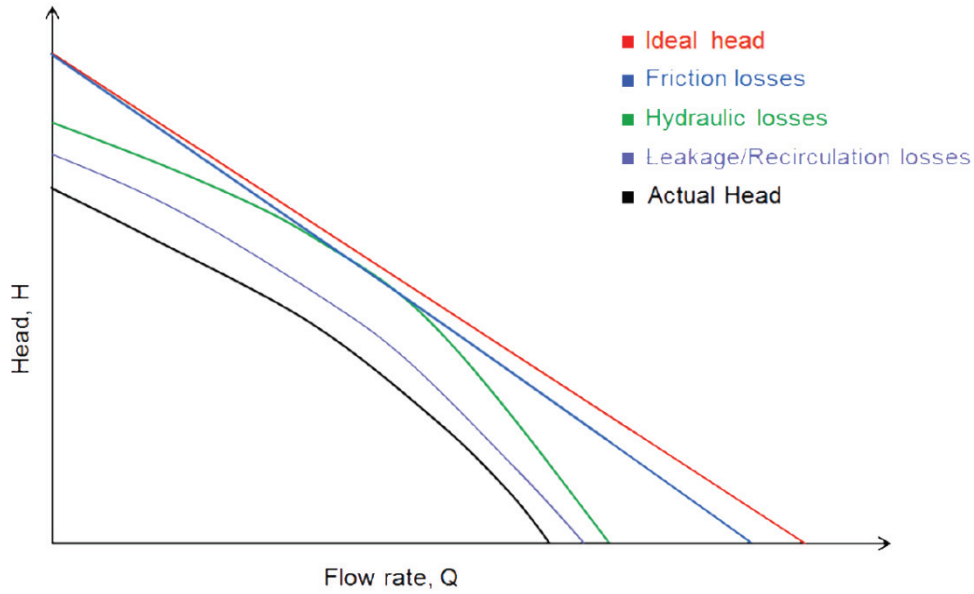
Figure 1.15 Losses affecting to pump head (Source: New Mexico Tech 2015)

1.5. Motivation of Thesis

This thesis concentrates on reducing the energy losses of a particular multistage centrifugal pump. When the effectiveness of that particular pump is considered, two main principles come into prominence:

- Pressure and tangential kinetic energy generation in rotating impeller.
- Pressure loss recovery in stationary guide vanes.

The correlation studies indicate that the pump geometry looks suitable and sufficient for the desired conditions in terms of pressure generation. The first stage of the investigated pump has a specific speed of 2700 according to the American dimension system and its vane geometry matchs up with the graph in Figure 1.4. It is mentioned by the pump manufacturer that the desired head gain is not as high as expected and this points to detailed impeller or return channel design is lacking. Upon this complaints, we decided to investigate this matter in detail with computational means. Initial CFD analysis showed that, recirculations and flow nonuniformities at the stationary section of the pump stages exist which block the water flow. As mentioned at

the previous chapter, this inefficiencies are part of the hydraulic losses and now it is seen that they are originated from the guide vane geometries.

Once the initial CFD studies are compeleted, it become obvious that focusing this study to the refinement of the pressure recovery section design by adjusting the guide vanes would benefit the most. According to the first simulation results which can be found in Chapter 3, no significant nonuniformities are observed at the rotating parts of pump stages. Therefore, it is decided that the problematic geometries, which are guide vane sections, are needed to be studied and fixed primarily.

CHAPTER 2

COMPUTATIONAL FLUID DYNAMICS

For many years, every engineering applications and designs have been validated by experiments. Although, experimental fluid dynamics (EFD) is still the most reliable technique for testing modified designs, it is time consuming and expensive. Especially in fluid dynamics, building experimental setups for complex cases needs overmuch effort. For this reason, Computational fluid dynamics (CFD) is developed with the advancing computer technology. CFD is a simulation technique which uses numerical approximations to solve necessary non-linear and coupled differential equations (namely Navier-Stokes Equations) according to the defined boundary conditions. This science can be interpreted as a combination of pure experiment and pure theory (Wendt 2009).

CFD has significant advantages compared to EFD (Damor, et al. 2013);

- It is cost efficient, since a physical setup is not required. Besides, there is no need for further expenses except initial hardware and software investment.
- Data can be precisely gathered at any point without measurement apparatus.
- It needs less manpower and time compared to experiments.
- CFD can handle most of the problematic cases without being affected from environmental and dangerous conditions.

Despite the effectiveness and practicality, there are some handicaps of using computational approach (Rangarajan 2013) (Denton 2010) ;

- Results may not reflect the predicted scenario, if the problem is not modelled well.

- Complex problems are needed to be run on powerful computers. Some engineerings problems, such as large Reynolds number turbulent flows, can not even be solved by the most powerful computers.
- It needs high knowledge of software and mathematics in order to model and understand even a simple simulation.

Even though CFD applications were started to be used in 1970's, modern CFD rises on the calculations of an English mathematician, Lewis Fry Richardson in early 1920's. In 1940's, his methodology is used on the first electronic computer ENIAC. After personal computers become widespread, CFD technology is improved incrementally (Hunt 1998) (Versteeg and Malalasekera 2007) (Khalil 2012).

CFD relies on solving differential equations by using numerical integration and/or differentiation methodologies. The fundamental equations that fluid dynamics rests on comes from the conservation laws of physics;

- conservation of mass
- conservation of momentum
- conservation of energy

In CFD language, these conservation principles are called governing equations and named, continuity, momentum, energy equation respectively (Blazek 2001) (Wendt 2009). Additional equations such as turbulence or transport equations can be added to these according to the type of the problem.

This study focuses on the flow behaviour of an incompressible fluid in steady state. Therefore, continuity and momentum equations are needed to be solved. Temperature changes are assumed to be unimportant and energy equation is not included. Simplified forms of continuity and momentum equations are written in Equations 2.1 and 2.2.

$$\nabla . (\rho \vec{v}) = 0 \tag{2.1}$$

$$\nabla . (\rho \vec{v} \vec{v}) = -\nabla p + \nabla . (\bar{\bar{\tau}}) + \rho \vec{g} + \vec{F} \tag{2.2}$$

CFD softwares may use different solution techniques to convert these differential equations into mathematical models. The reason of this conversion is to create matrices which can be manuplated by computers (Bhaskaran and Collins 2002). There are three techniques that are widely used for this purposes;

- Finite Difference Model (FDM)
- Finite Element Model (FEM)
- Finite Volume Model (FVM)

Nowadays, FEM and FVM are used in most of the CFD softwares. Each of these three methods are suitable for different type of analysis. For instance, FDM is preferred for the applications that require higher order accuracy, as meteorological and aerospace implementations, since it is the most direct method of all. However, in most of the engineering applications, due to the geometrical complications, FEM and FVM are used. All of these techniques separate the physical space into subdivisions which are finite-sized elements with simple geometries that are called cells. In FEM, governing equations are implemented for each element, therefore the computational effort becomes much in spite of high rate of accuracy. This method is employed mostly for structural analysis when it is introduced, but it is also used for CFD analysis nowadays by several commercial softwares. As for FVM, this method is specialized for CFD since the conservation can be guaranteed for each cell. Unlike FEM, FVM deals with only the conservation terms at the cell boundaries. Thereby, handling continuous media and nonlinear problems are not difficult compared to other methods (Sjodin 2016).

2.1. CFD for Turbomachinery

Turbomachinery term represents the energy conversion between a rotating machine and fluid (Pinto, et al. 2016). Turbomachinery flows are one of the most complicated and troublesome flows in fluid dynamics because of the complicated geometries, three dimensional nature of the flow, and virtual forces created by rotating reference frames.

CFD usage for simulating turbomachinery flows has increased in recent years with developing computer power technology (Aghaei tog, Tousi and Tourani 2008).

From 1980s to 2011, capabilities of commputers increased 25 times (Jameson 2012). As a result of this, more and more accurate solutions for off-design conditions or highly separated flows are being needed. Especially, it has been a necessity to handle turbulent flows accurate enough. Several transport equations have been derived and different turbulence models have been developed by researchers for this purposes. However none of these models are valid for all applications. Therefore, it is required to use the most suitable method for the problem at hand in order to have an accurate result (Zhou and Shi 2012)

2.1.1 Turbulence models

In turbomachinery simulations, standart two equation models are the most common and validated turbulence models (Tao, et al. 2014) (Li and Wang 2007). As an example, k-ε model assumes a fully turbulent flow and neglects the unisotropic effects. As a result of this, it is good for solving turbulent flows in far away from the walls where shear and unisotropy becomes unimportant. Distinctively, k-ω model uses specific dissipation variable(ω) instead of dissipation rate(ε) and involves the turbulent viscosity term(μ_t) into transport equations. Therefore, k-ω model becomes more appropriate for boundary layer regions and its transport equations are given in Equation 2.3 and 2.4.

$$\frac{\partial}{\partial x_i}(\rho k u_i) = \frac{\partial}{\partial x_j}\left(\Gamma_k \frac{\partial k}{\partial x_j}\right) + \bar{G}_k - Y_k \tag{2.3}$$

$$\frac{\partial}{\partial x_i}(\rho \omega u_i) = \frac{\partial}{\partial x_j}\left(\Gamma_\omega \frac{\partial \omega}{\partial x_j}\right) + \bar{G}_\omega - Y_\omega + D_\omega \tag{2.4}$$

$$\omega = \frac{\varepsilon}{k} \tag{2.5}$$

$$\mu_t = \rho\left(\frac{k}{\omega}\right) \tag{2.6}$$

Although, both of these models do their jobs, a big problem of predicting the flow behaviour approaching the wall region can not be completely cleared up. Resulting

from the lack of solution methods, Menter developed Shear Stress Transport (SST) k-ω model which is a combination of standart two equation models.

The effectiveness of the new model is the modulation of the general equation according to the blending function, F_1. Equation 2.7 shows the blending of two model equations by Menter.

$$\emptyset = F_1\emptyset_1 + (1 - F_1)\emptyset_2 \qquad (2.7)$$

The blending function, F_1 becomes 1 inside the boundary layer and 0 in the free stream. In the blending equation, $\emptyset$, $\emptyset_1$, $\emptyset_2$ represent the new model, original k-ω and standart k-ε models respectively. As a result of this concept, k-ω model is used for near-wall regions and k-ε model is stepped in for free shear zones. Hence turbulence equations are solved in best efficient way

This new model is named as Baseline model, (BSL). However, in this model, wall shear stress is too high and flow does not separate from smooth surfaces correctly. Menter implements the Bradshaw's assumption to BSL model. According to Bradshaw, the shear stress in boundary layer is proportional with the turbulent kinetic energy as;

$$\tau = \rho a_1 k \qquad (2.8)$$

where a_1 is SST closure constant, act as a viscosity limiter. After these modifications, k-ω SST model provides a solution for the weaknesses of two equation models. (Menter 1994).

The Figure 2.1 below validates the effectiveness of the k-ω SST model by comparing with different turbulence models' simulations and experimental data. Menter's work aims to compare the standart turbulence models and new developed models by investigating an airfoil flow. Figure 2.1a and 2.1c shows that the pressure distribution on the airfoil surface and velocity profiles match with the experimental data. This confirms the statement that k-ω SST model has a better flow separation prediction capability compared to standart models. In Figure 2.1b and 2.1d, it is expected that shear stress prediction of k-ε turbulence model is weak due its characteristics. However, k-ω SST model also comes into prominence of all ω-based models in shear stress computations.
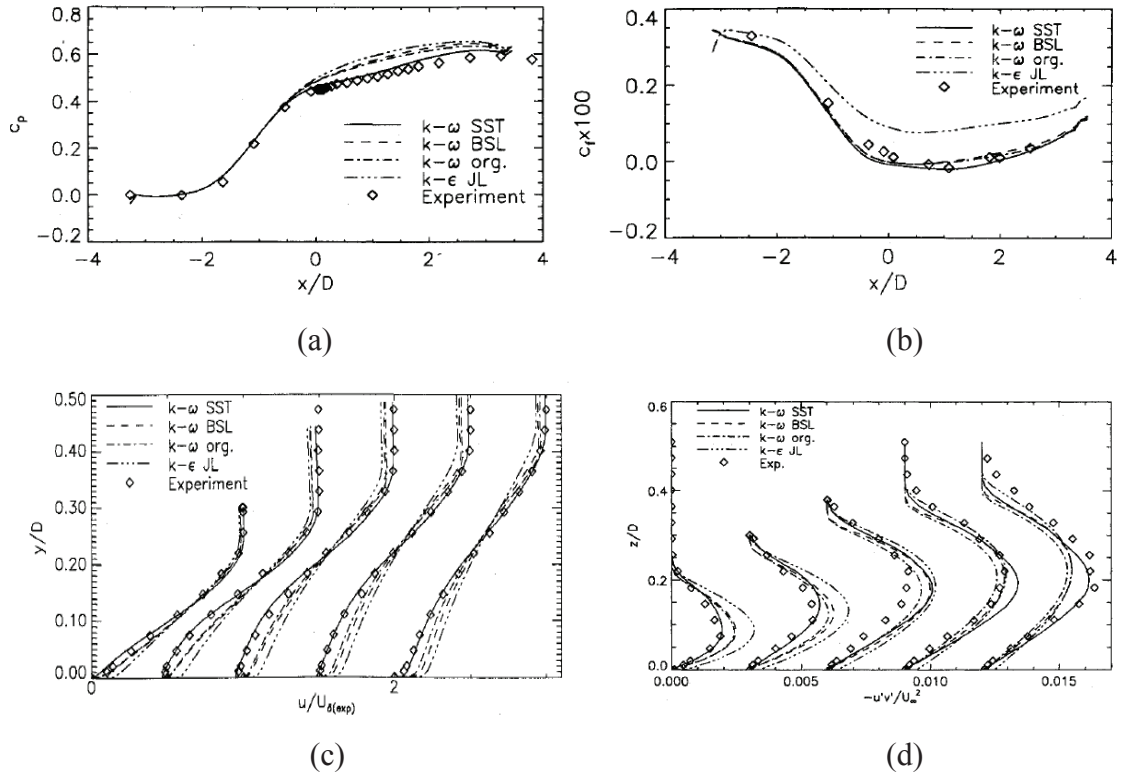
Figure 2.1 Comparison of different turbulence model simulations and experiment
(Source: Menter 1994) (a) Wall pressure distribution, (b) Wall shear stresses,
(c) Velocity profiles, (d) Turbulent shear stresses

CHAPTER 3

ORIGINAL MODEL AND SIMULATIONS

This chapter of the thesis investigates the characteristics, design methods, numerical analysis of a 5-stage electrical submersible pump and all of the studies are made according to the solid model of manufactured product.

3.1. Impeller Geometry

As mentioned in the previous chapters, impeller is the heart of a centrifugal pump. In order to have a uniform flow in impeller channels, flow area and vane number should be adjusted in the basis of design requirements. Geometric specifications of current impeller design is given in Table 3.1. Impeller diameters and angles are shown in Figure 3.1 and Figure 3.2 respectively.
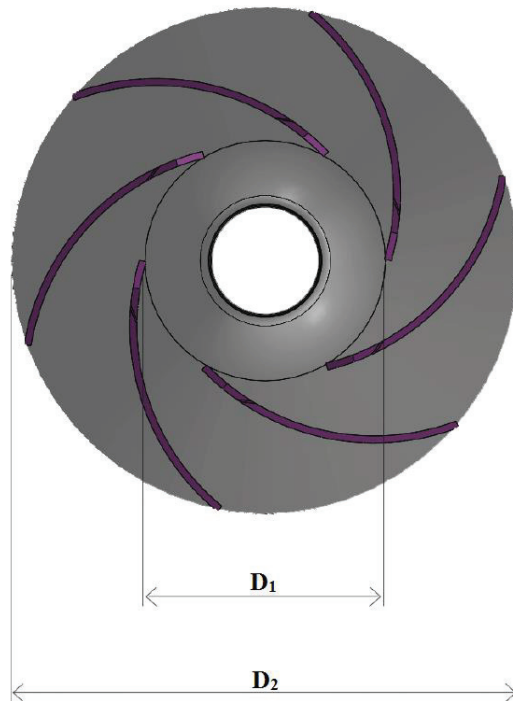
Figure 3.1 Top view of original impeller geometry
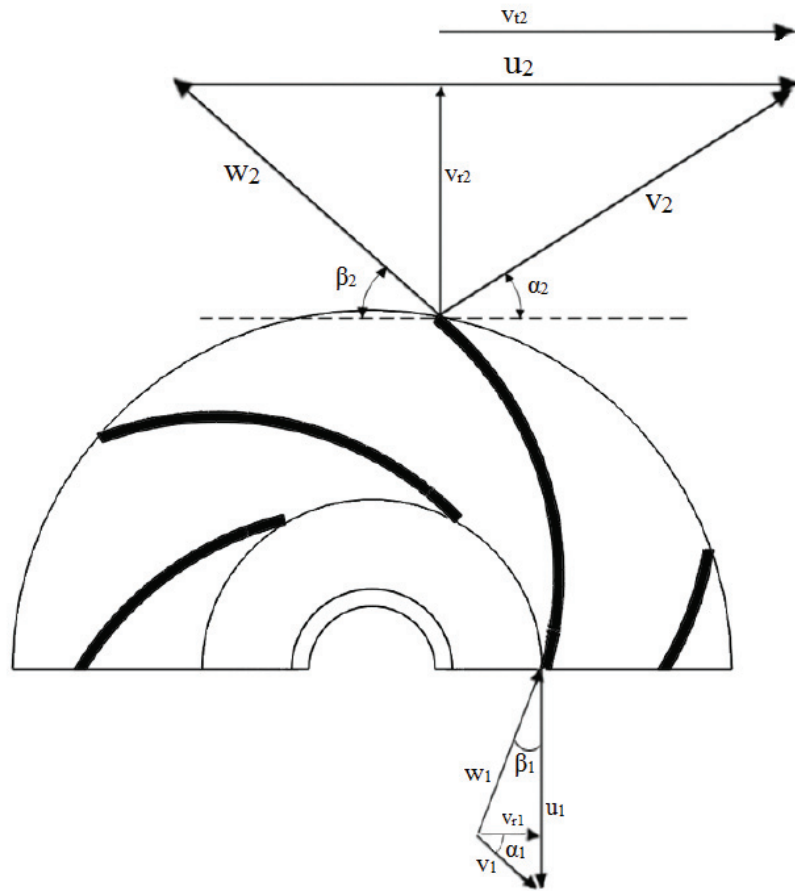
Figure 3.2 Impeller blade angles and velocity triangles

The flow outlet angle in Table 3.1 is calculated according to the velocity triangles. Step by step calculation can be found in Appendix A.

Table 3.1 Geometric properties of original impeller

Blade Number	6
Impeller Diameter (D_2)	73 mm
Impeller Eye Diameter (D_1)	34 mm
Blade Inlet Angle (β_1)	17°
Blade Outlet Angle (β_2)	28°
Flow outlet angle (α_2)	11°

Several blade design methods are used to obtain the required head. In the original design made by the manufacturer, simple arc method (SAM) is applied for shaping the impeller vanes. Although it is hard to access to step by step methods for

impeller vane geometry, SAM, double arc method (DAM) and the similar curvature design methods are explained by Kyparissis clearly (Kyparissis, et al. 2009) (Bowade and Parashar 2015). Figure 3.3 shows the vane profiles which are drawn according to SAM and DAM. It can be seen that manufactured design and SAM drawing are matching perfectly.
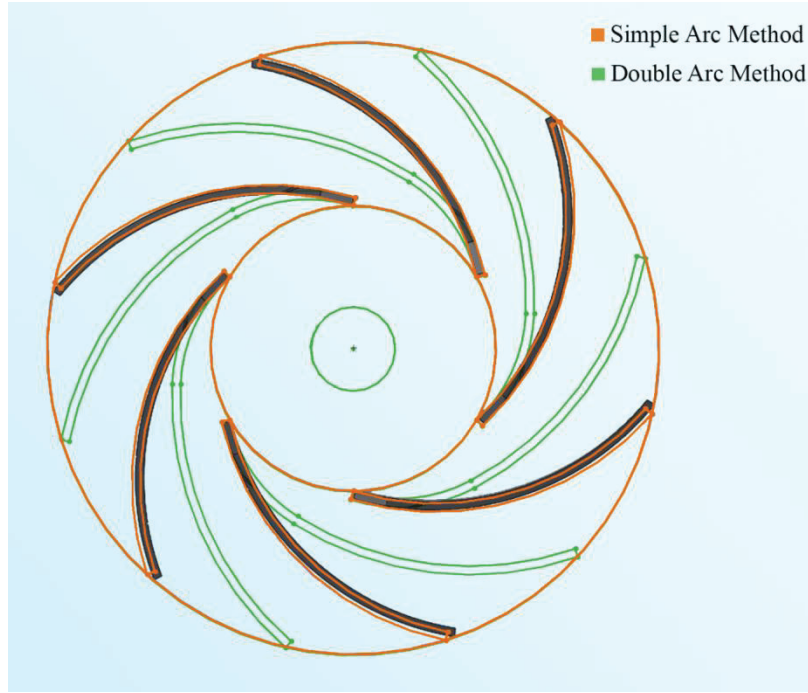
Figure 3.3 Different Impeller design methods

3.2 Return Channel Geometry

Stationary elements have a critical effect on stage efficiency, since they are the energy recovery components of a turbomachinery. The geometric parameters of guide vane design are; vane inlet angle, outlet angle, wrap angle and vane number. The performance parameter is the pressure loss coefficient which is the ratio of total pressure loss to inlet dynamic pressure and wrap angle defines the arc between the projections of initial and end points of a vane (Turunen-Saaresti 2004) (Lee, et al. 2016).

$$\xi = \frac{P_{t_2} - P_{t_3}}{P_{t_2} - P_{s_2}} \tag{3.1}$$

24

Pressure loss coefficient formula can be seen in Equation 3.1 where P_{t_2} and P_{t_3} is total pressure at return channel inlet and outlet respectively, P_{s_2} is the static pressure at channel inlet.

Table 3.2. Properties of original return channel

Vane Inlet Angle (ϕ_1)	39°
Vane Outlet Angle (ϕ_2)	90°
Wrap Angle (θ)	40°
Vane Number	8

Design parameters of the manufactured return channel blades are shown in Table 3.2 and vane angles are indicated in Figure 3.4.
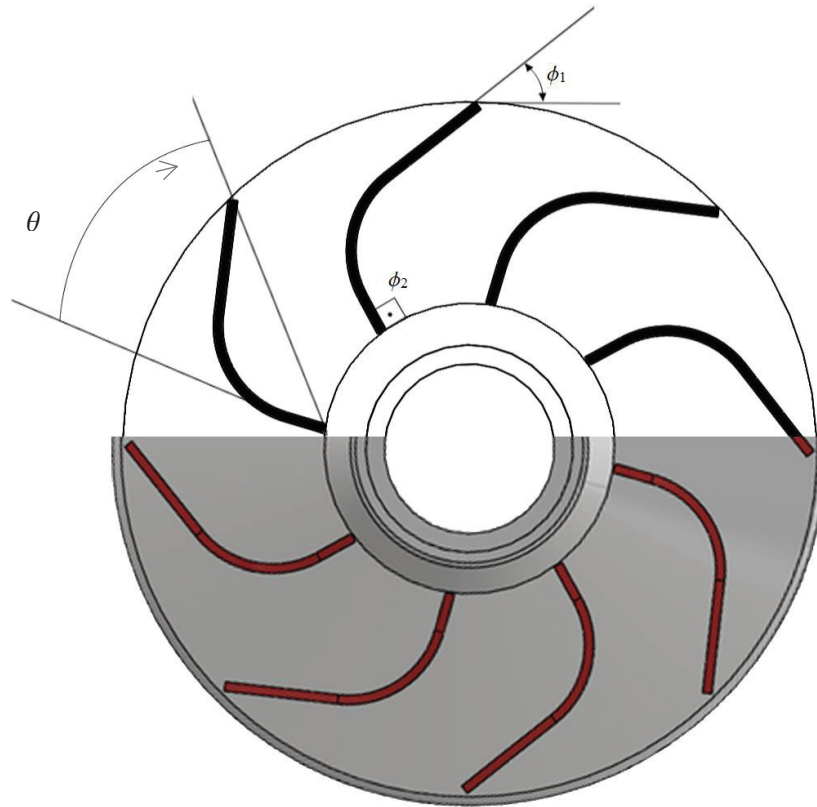
Figure 3.4 Top view of the original return channel and guide vanes with angles (as it comes from the manufacturer)

3.3. CFD Analyses

In this study, numerical analyses are handled with ANSYS Fluent CFD software. In order to run the simulation, flow domain has to be created. There are several modules for converting 3D solid model into the fluid domain in ANSYS Workbench. However, for this case SolidWorks CAD software is preferred for major applications because of its ease of use.

Stage	Activity
Initial Data	• Gathering Geometric Data
CAD Software	• 3D Modelling
Design Modeler / Space Claim	• Geometry Cleaning • Preparing for Meshing
Meshing	• Grid Generation
Fluent Launcher	• Processing Options
Solver	• Setting up Flow Characteristics and Governing Equations (material, boundary conditions, solution methods)
CFD-Post	• Simulation Results (contours, streamlines, vectors)

Figure 3.5 Steps of CFD simulation from manufactured product to result visualisation

3.3.1 Fluid Domain Creation

In CAD model, components of the existing pump are nested. It is not a suitable geometry for turbomachinery simulations, since rotating and stationary zones should be defined separately.

Figure 3.6 Nested components of manufactured pump stage

So as to create the experimental domain, rotor and stator zones are modelled individually. Boundaries of the domain is determined according to the wet surfaces and the flow path which is demonstrated in Figure 3.7.
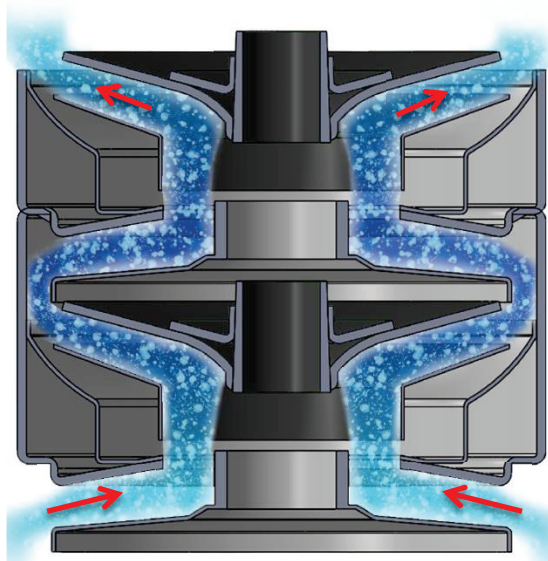
Figure 3.7 Demonstration of flow through inpeller and guide vane channells

Then, impeller blades and guide vanes which were designed by manufacturer are extracted from filled bodies (Figure 3.8a, 3.8b) and assembled in the way that fluid can travel as in Figure 3.7. Additionally, two extension pipes whose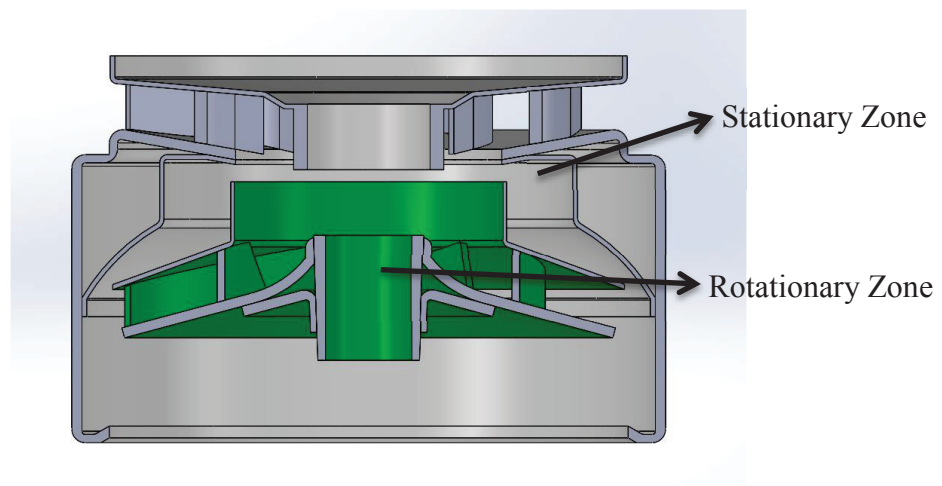 lengths are 3D and 6D are attached to inlet and outlet respectively. These pipes are crucial in order to diminish the boundary condition effects and obtain accurate results. The computational domain of 5-stage pump is shown in Figure 3.8c.

(a)   (b)

(c)
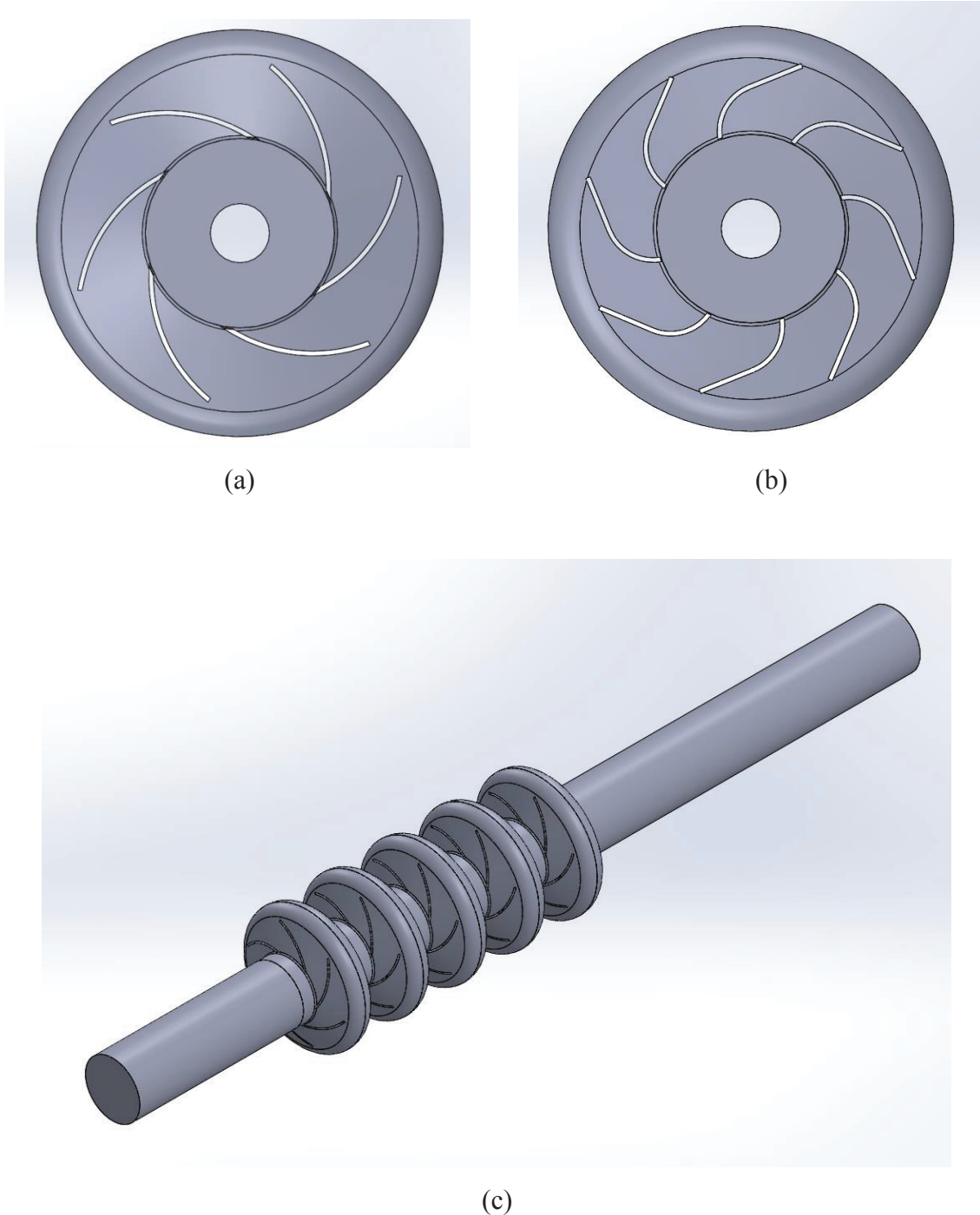
Figure 3.8 Fluid domain model (a) Top view of impeller zone, (b) Top view of guide vane zone, (c) Isometric view of five stages with extension pipes.

During modelling, small features such as fillets, mating faces are not taken into consideration. Since they do not make notable effects on flow performance and CFD softwares consume a lot of computational effort while handling them, they have been decided to be simplified. The images in Figure 3.9 are two examples of small features. Both, fillet and mating rings are modelled for the reason of manufacturing and they are not involved to the flow. Therefore, these kind of features are not included when creating the fluid domain.
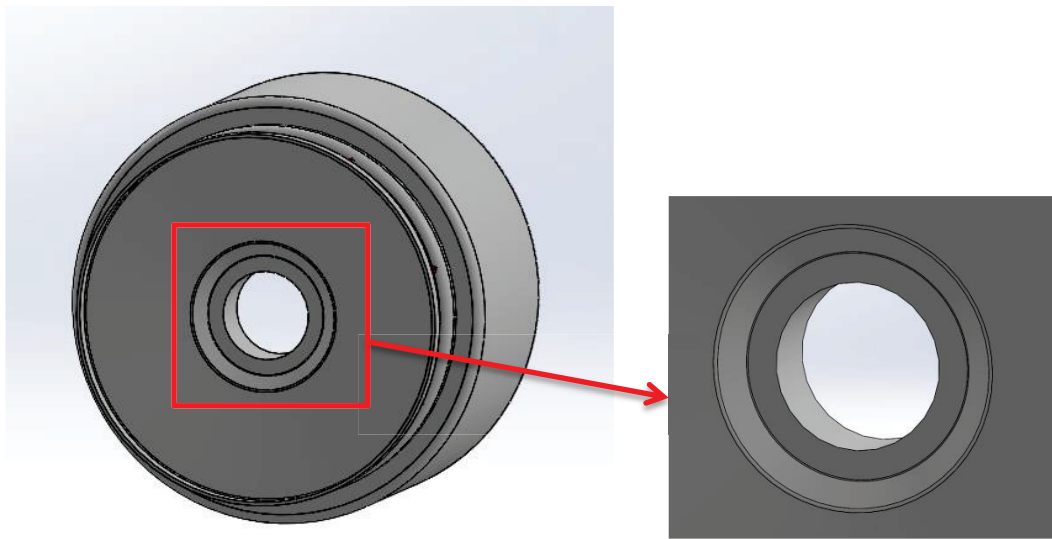
(a)
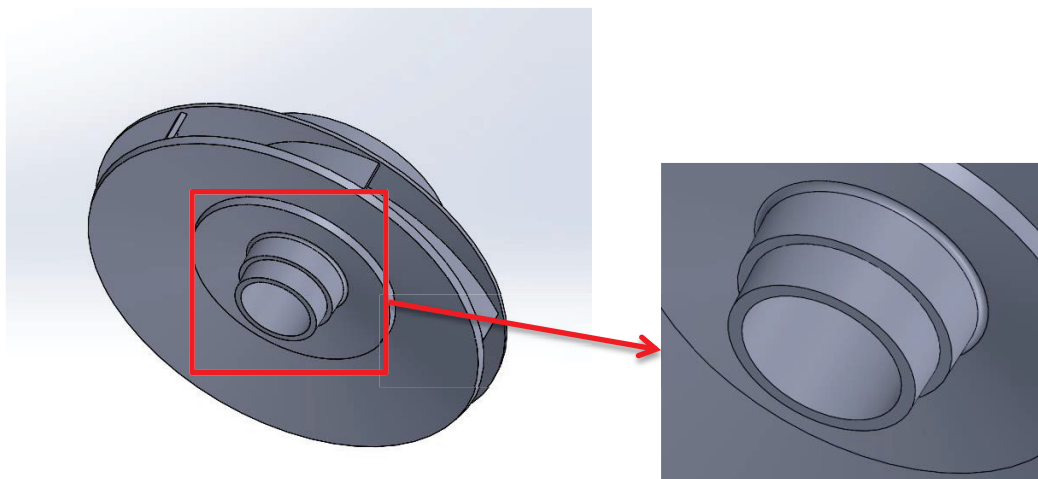
(b)

Figure 3.9 Examples of small features

3.3.2 Meshing

Solving governing equations for monolithic geometries is not possible except very simple cases. Therefore, the created geometry is divided into smaller subdomains called cells and corners of cells are called nodes. Cells create a network called mesh which represent the computational domain.

Since the grid with smaller element size covers more detail about flow characteristics, mesh element number is directly proportional with the solution accuracy until the mesh independency is reached. On the otherhand, as the element number increases, required computer memory and solution time also increase. So as to determine the optimum element number and size, mesh independency test is needed. Besides, in a desired mesh, smaller size of elements should be assigned for the sections in which flow disturbances may occur such as edges, curvatures, extractions or contractions. In order to control the mesh size, Ansys Meshing offers size functions.

In this study, curvature based and proximity based size functions are used to determine the mesh size. Proximity size function arranges the mesh size according to the closeness of source boundaries which are edges and faces. For narrow passages such as the flow between vanes, proximity function is useful to create the grid. As it is seen in Figure 3.7 that flow enters L-bends and U-bends while travelling through stages. In these curved passages, curvature based size function computes mesh sizes according to the specified curvature angle.
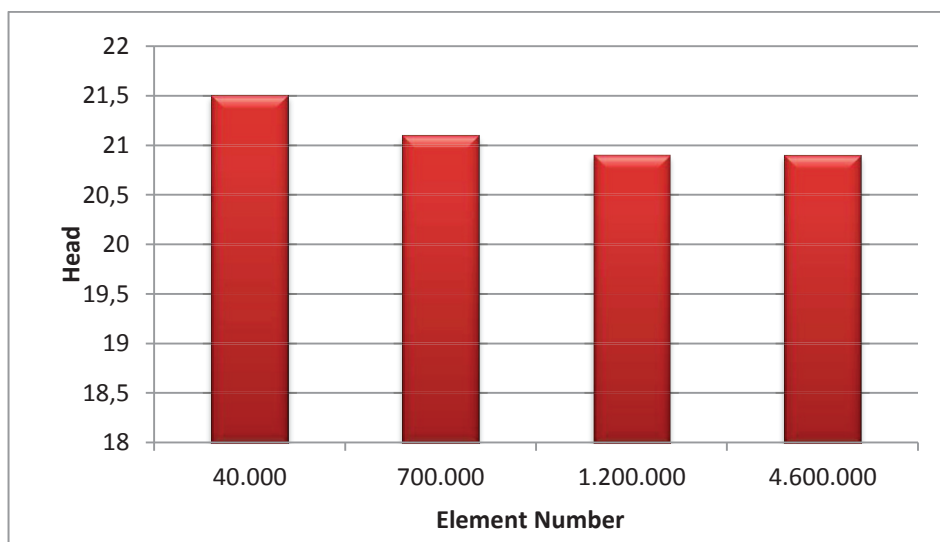
Figure 3.10 Mesh independency test

As can be seen in Figure 3.10, solution becomes independent of element number for the grids with more than 1 million cells. Therefore, fine meshing gives reliable results in shorter time. Head parameter is chosen in order to observe the independency, since, it gives an opportunity to check the trueness of the simulation by comparing with the experimental data which the manufacturer provides.
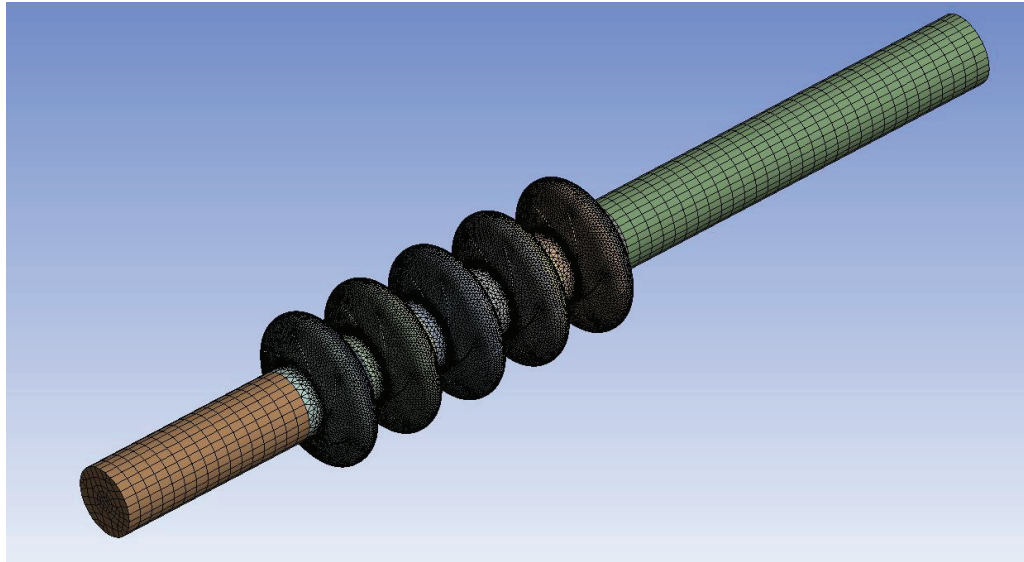
(a)
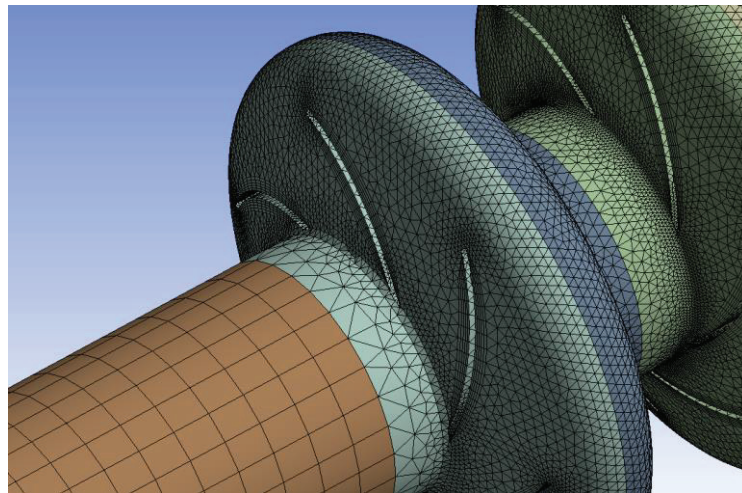
(b)

Figure 3.11 Computational domain mesh.

Mesh network can be seen in Figure 3.11a. The size difference between zones is resulted from different size functions. The average mesh si sizes of stages and extension pipes are adjusted as 2mm and 5mm respectively. In Figure 3.11b, the difference is seen

more detailed. Elements are formed smaller in vaned areas due to the proximity function. Mesh size may get small down to 0.25 mm for vane tips and bends because of the effect of curvatures.

When handling turbulent flows between walls, shear effects become more important. Average tetrahedral meshes are good at solving pressure field, but it is needed to increase the mesh quality at near wall regions because of the high shear rates.

As for the boundary layers, according to Schlichting, viscous effects are observed in three regions (Schlichting and Gersten 2017). Therefore, when generating the boundary layer mesh, cell size should be adjusted due to the y^+ value which is a non-dimensional distance between the wall and first node.

viscous sublayer	$0 \leq y^+ \leq 5$
buffer layer	$5 \leq y^+ \leq 70$
overlap layer	$70 \leq y^+$

Since the near wall region of the boundary layer will be modelled by a wall function, first cell should not be in this layer. Early trials with Ansys suggest that this fist cell should not be placed in $5 \leq y^+ \leq 30$. Therefore, in this study y^+ value is taken as 30 and therefore, the first cell height became 0,1 mm.
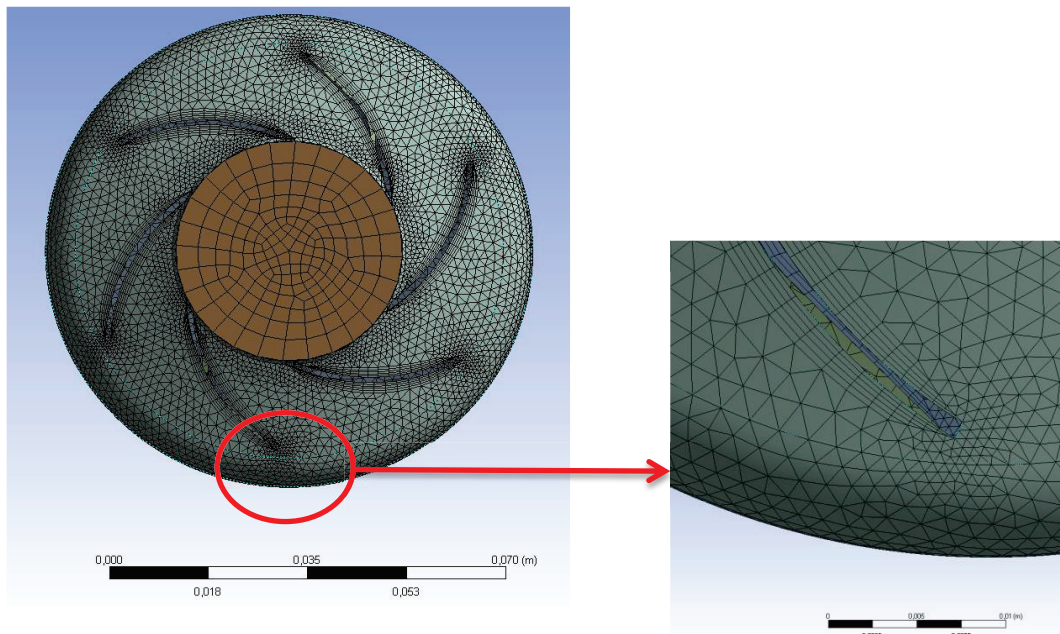

Figure 3.12 Boundary layer mesh near impeller blades.

3.3.3 Solver Settings

CFD softwares have several solution techniques for handling different type of problems. In this study, flow behavior is investigated in a steady state. Transient simulation is not preferred because of its high computational effort requirement and the pump efficiency problem is mostly a steady problem. A problem, on the other hand, such as impeller-diffuser interaction would have require a transient solution.. Besides, pressure-based solver is implemented instead of density-based solver since the water flow is basically incompressibile (Sankaran and Merkle n.d.).

Computational domain consists of both rotating and stationary regions which share a common surface Due to the steady simulation and the weak interaction between cell zones, a multiple reference frame (MRF) method is preferred instead of a translational method which is more advantageous for transient simulations and close blade to blade interactions such as impeller-diffuser cases (Modeling flows in moving zones 2013). Implementing the MRF method to describe the motion is the simplest way when handling with cell zones with different rotational speeds in steady-state simulations (Oshinowo, et al. 2000).

In MRF method, governing equations are written with respect to the reference frame of each cell zone. As a result of this, conservation equations of stationary and moving cell zones are governed distinctively. However, Fluent software uses absolute velocity values to make calculations correctly for all neighbour subdomains. Therefore, the velocity terms in the moving zones have to be converted from relative reference frame to absolute frame by using the relation;

$$\vec{V_r} = \vec{V} - \vec{u}_r \qquad (3.2)$$

Where $\vec{V_r}$ is the velocity in the moving frame, $\vec{V}$ is the absolute velocity and $\vec{u}_r$ is the velocity of the moving frame relative to the inertial reference frame (ANSYS Inc. 2013).

Boundary condition definition is the key point of a CFD simulation for adapting the desired behavior of fluid. In this thesis, investigated property is the total head which is obtained by the pressure difference between inlet and outlet boundaries of the domain. ΔP is generated by the transfer of angular kinetic energy to working fluid.

Figure 3.13 shows the boundaries of the computational model and conditions are defined based on assumptions and pump characteristics. It is assumed that the pump operates in ditch water at fluid level, so it is accepted that the total pressure at the inlet boundary is 0 Pa. When defining the outlet boundary conditions, pump capacity at the best efficient point is based on and 8 tons/h which is 2,222 kg/s of outlet flow is accepted. Although, there is not any solid bodies in computational domain, wall conditions which force the outer surface to move with the cell zone are assigned for rotational parts of domain.
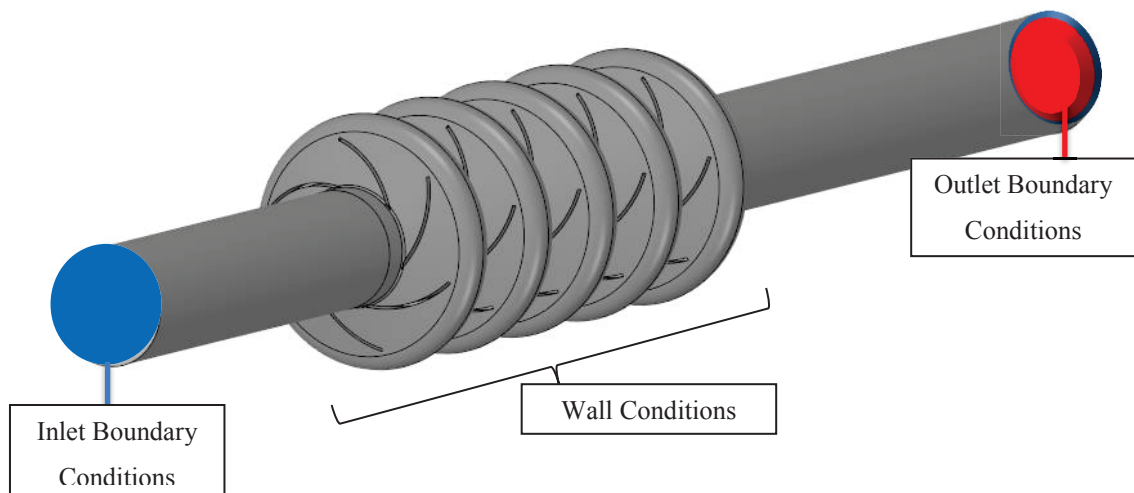
Figure 3.13 Demonstration of boundary conditions on fluid domain

3.3.4 Simulation Results

A tipical total pressure development along a 5-stage pump is shown in Figure 3.14. It indicates that the flow development is in the desired manner. It is inferred clearly from the color changes, total pressure of the fluid increases through stages. The bar chart in Figure 3.15 shows the contribution of each stage with respect to the total pressure gain. There is not any significant difference between stages, this means each stage affect the pressure rise equally as it should be.

Figure 3.14 Pressure generation through stages

Figure 3.15 Pressure generation of each stage

As it is stated at the beginning of Chapter 2, one of the advantageous features of CFD softwares is to visualize the flow behaviour at each point. This helps to understand the flow problems and its locations easily.
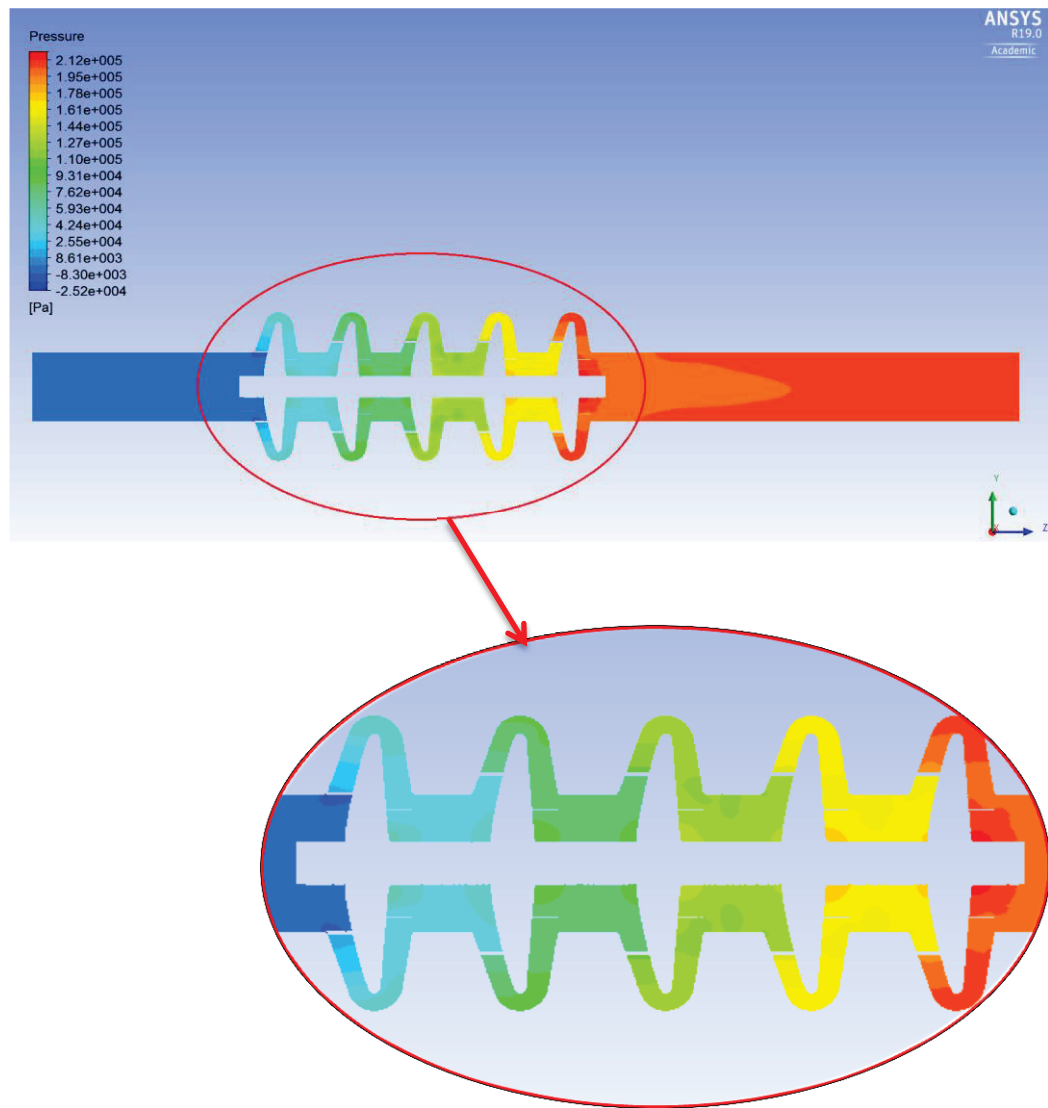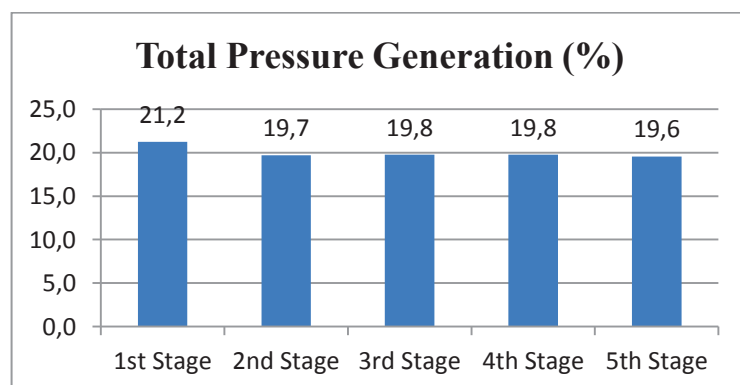
In Figure 3.16, velocity streamlines at impeller section are shown. It can be seen that, the relatively uniform flow is seen between the impeller blades is not similarly observed between guide vanes. Small, but important, swirls occuring at pressure sides on the guide vanes can clearly seen in the figure 3.17. These swirls block the free flow area and therefore create energy loss and affect pump head directly. As it is understood from the locations of the swirls, the main reason of this is the sharp curved geometry of the guide vanes.

Apart from the streamline visuals, the performance parameters for best efficient point of 5-stage model are shown in Table 3.3.

Table 3.3 Performance parameters of original design

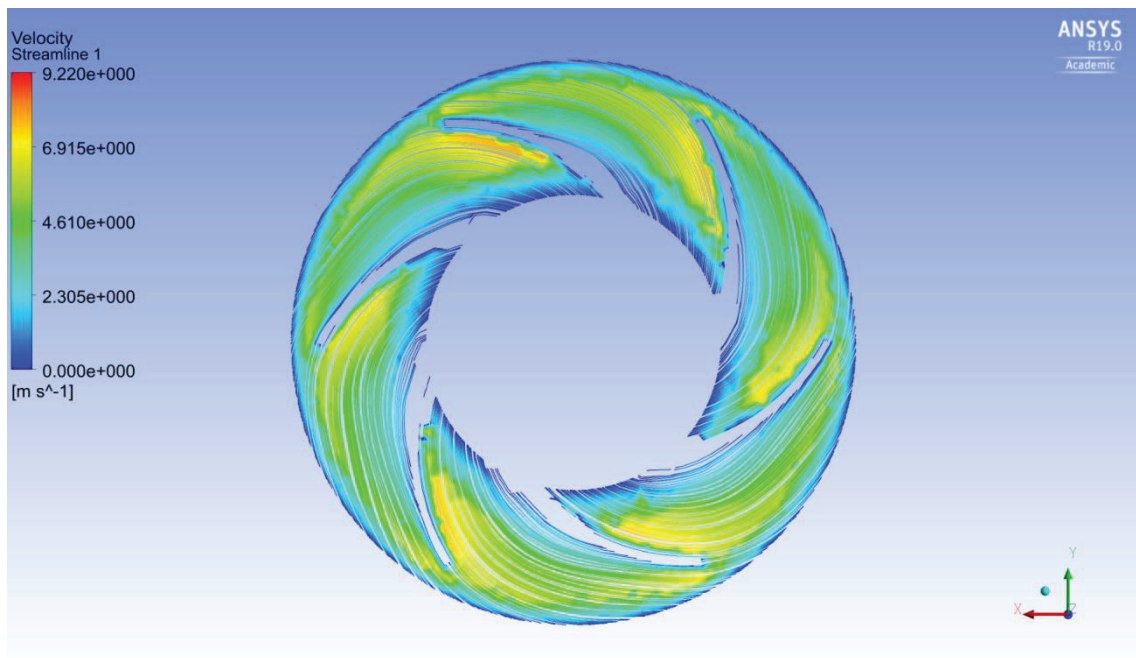| Total head (m)	21.6
Hydraulic efficiency	0.63
Loss coefficient	0.92

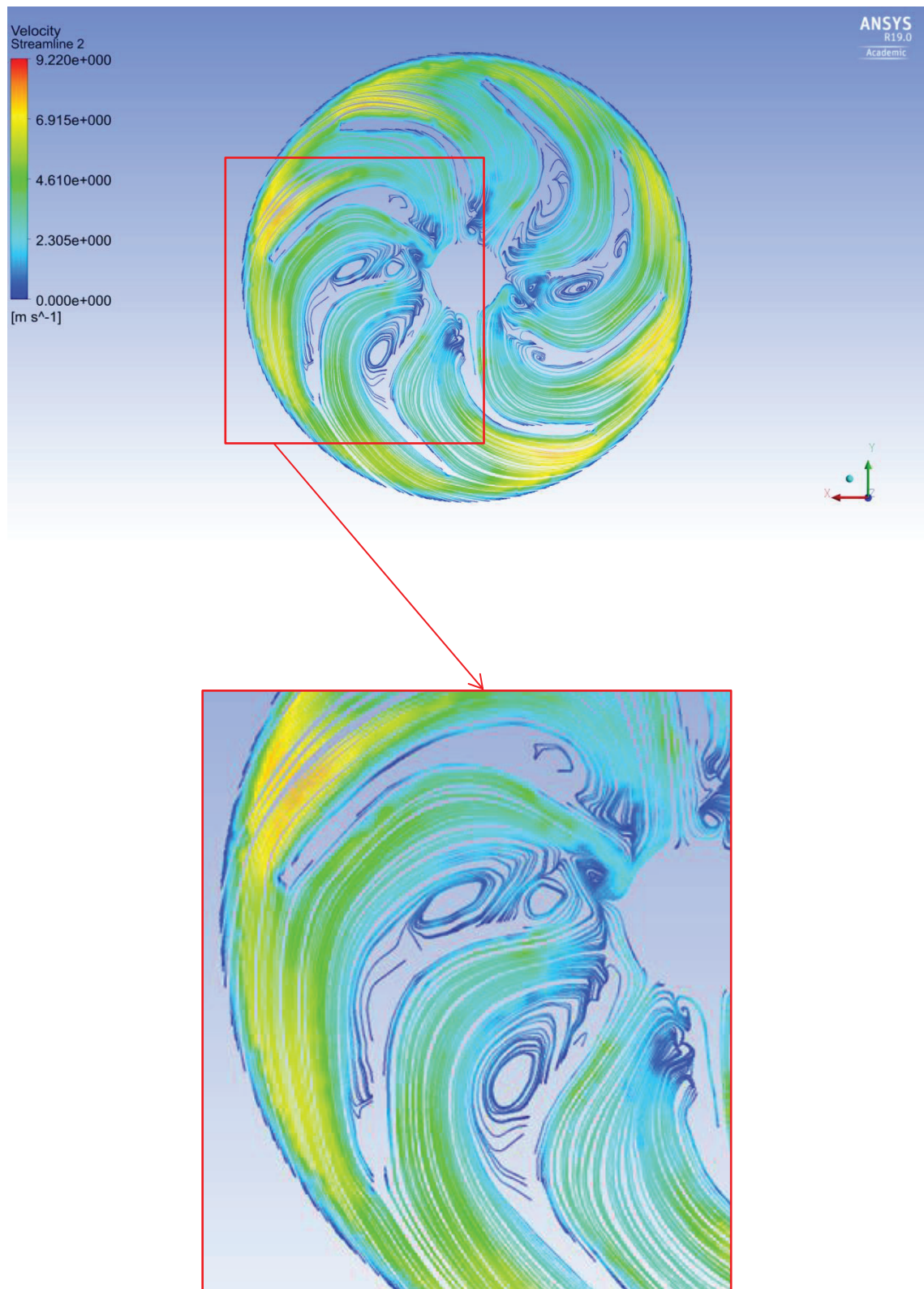Figure 3.16 Velocity streamlines of original design at impeller section

Figure 3.17 Velocity streamlines of original design at guide vane section

CHAPTER 4

MODIFIED DESIGN AND SIMULATIONS

As referred in previous chapters, hydraulic efficiency of investigated pump is determined by two main components. Geometry of impeller blades and guide vanes affects the velocity profiles and produced thrust directly. In consequence of previous simulations, it can be seen that guide vane section is the main reason of the inefficiencies for the manufactured pump. It is clearly seen in Figure 3.16 and Figure 3.17 that, the uniform flow between impeller blades do not last in the guide vane section due to their badly designed geometry. This chapter of the thesis aim to clear away the loss producing entities and increase the efficiency of the pump.

4.1 Modified Guide Vane Design

Considering the early studies on pressure recovery in stationary parts of centrifugal pumps, several parameters which affects the hydraulic efficiency come forward. These are vane inlet and outlet angles, curvature profile and wrap angle.

Guide vanes are located after the rotationary zone to recover the tangential kinetic energy which has a potential to turn into loss. In order to minimize the energy dissipation through stages, the guide vane inlet angle and the velocity vectors at impeller outlet are needed to be aligned (Shi, et al. 2009).

Bian's study verifies the need of angle alignment. He created a freestream flow of 25 degrees and simulated two different cases with blade angles of 15 and 30 degrees. He observed the flow behaviour after blade tips and calculated the loss coefficients for two different velocities. In Figure 4.1a, it is clearly seen that the flow tends to separate when it meets with the blade of 15 degrees. The graph in Figure 4.1c shows that, the minimum loss is gained between 25 and 30 degrees which is very close to the freestream flow angle.
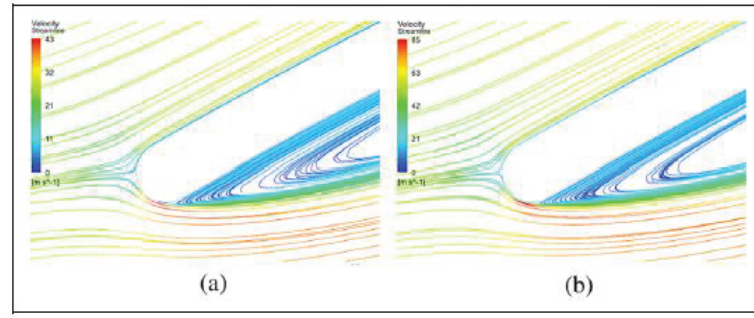
(a)
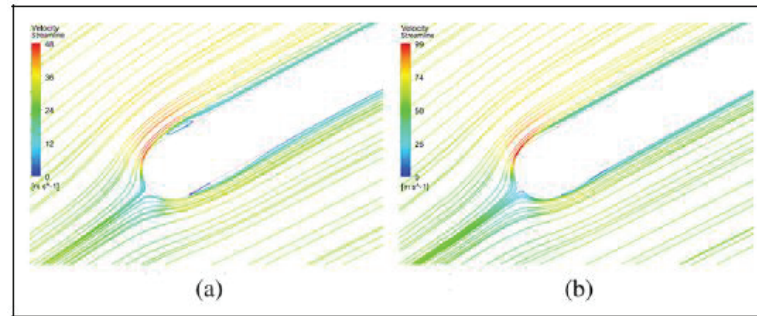
(b)
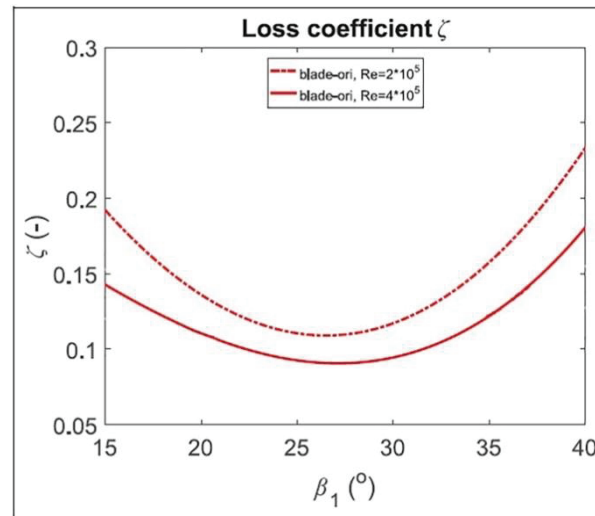
(c)

Figure 4.1 Demonstration of flow and blade angle alignment (Source: Bian, 2018) (a) β2= 15° (b) β2= 30° (c) Loss coefficients

According to the velocity triangles at the tip of impeller blades in Figure 3.2, it is seen that α_2 angle is 11 degree. However, Table 3.2 indicates that guide vane inlet angle of manufactured pump, ϕ_1 is 39 degree. This incompatibility may cause entrance shock losses.

In centrifugal pumps, flow enters to impeller eye radially and leaves through impeller blades partially radial partially tangentially. Therefore, it is desired that the upcoming flow enters to next stage without tangential component. Guide vane outlet angle ϕ_2 affects this behaviour directly by forcing the flow to counter swirl. It has shown that when guide vane outlet angle is in a range from 90 to 100 degrees, the pump efficiency is maximized for best efficiency point (Lee, et al. 2016).

The main reason for the recirculation at the pressure side is the sharp curved geometry of the vanes. In order to eliminate the recirculation losses, vane incidence angle should be increased gradually. Figure 4.2 indicates the curvature profiles of guide vane designs by using combs and Figure 4.3 demonstrates the vane profile.
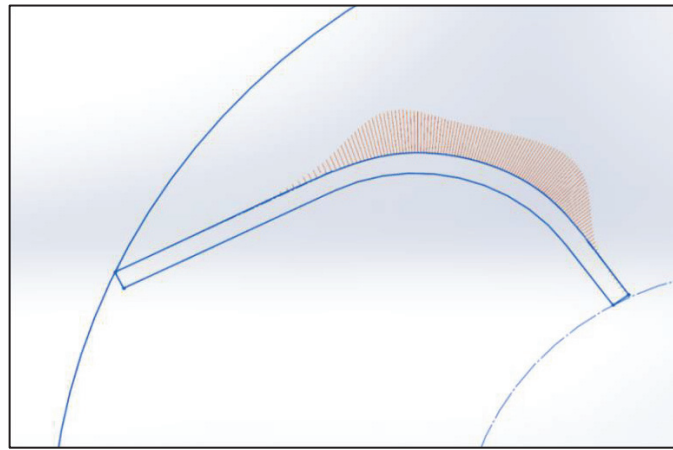
(a)
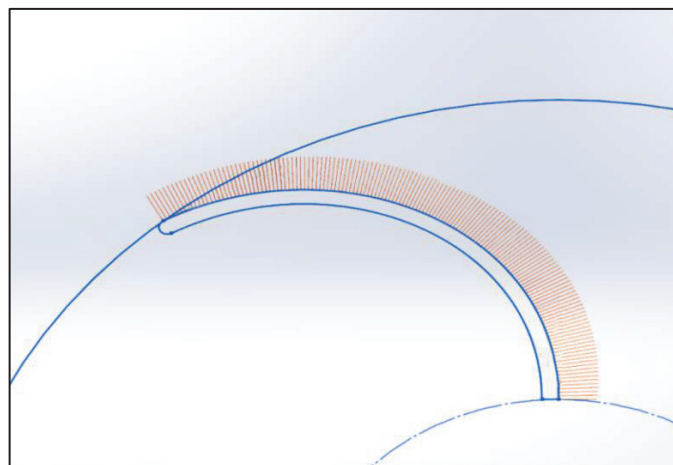
(b)

Figure 4.2 Curvature combs of guide vane sketches (a) Original design, (b) Modified design
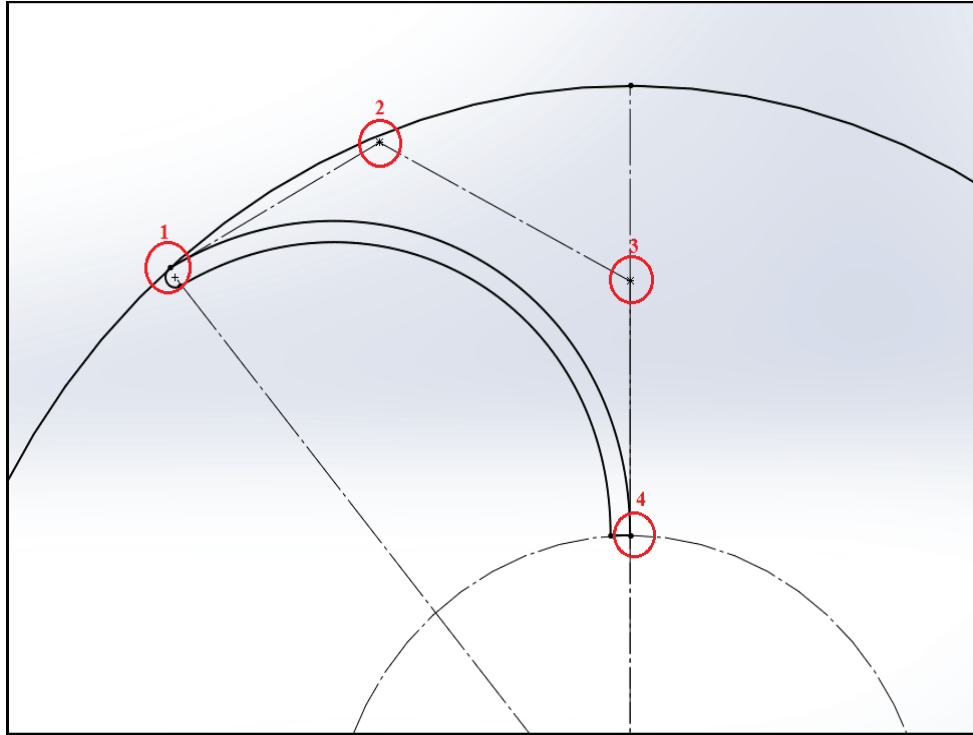
Figure 4.3 Guide vane profile and control points

In vane design procedure, 3rd degree Bezier curve is used. Four control points are fixed according to leading edge, inlet angle, exit angle and trailing edge respectively. Positions of point 2 and point 3 are adjusted in the manner that the curvature combs distribute on vane area equally.

Apart from this, Aungier's studies recommend that the ratio of flow passage width and mean streamline curvature radius should be below 1 for local values and 0.8 for crossover bend section (Aungier 2000). Table 4.1 and Figure 4.4 shows the dimensions of new return channel where, R is mean streamline curvature radius, b is channel width at L-bend and b_C is channel width at crossover bend. In modelling period, return channel is designed considering these recommendations. The reason of measuring the chanel width at L-bend is that it is the widest part of the passage.

Table 4.1. Width to curvature ratios for guide vane channel

R(mm)	b(mm)	b_C(mm)	b/R	b_C/R
7,80	7,62	5,76	0.97	0.73
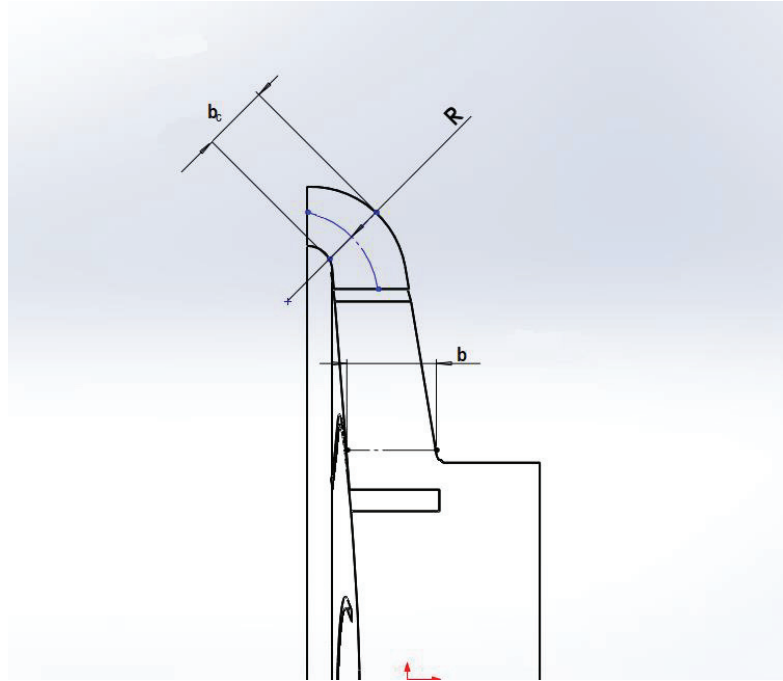
Figure 4.4 Meridional view of return channell

Considering the angle alignments and curvature profile modifications of the new guide vane design, the solid model can be seen in Figure 4.5.
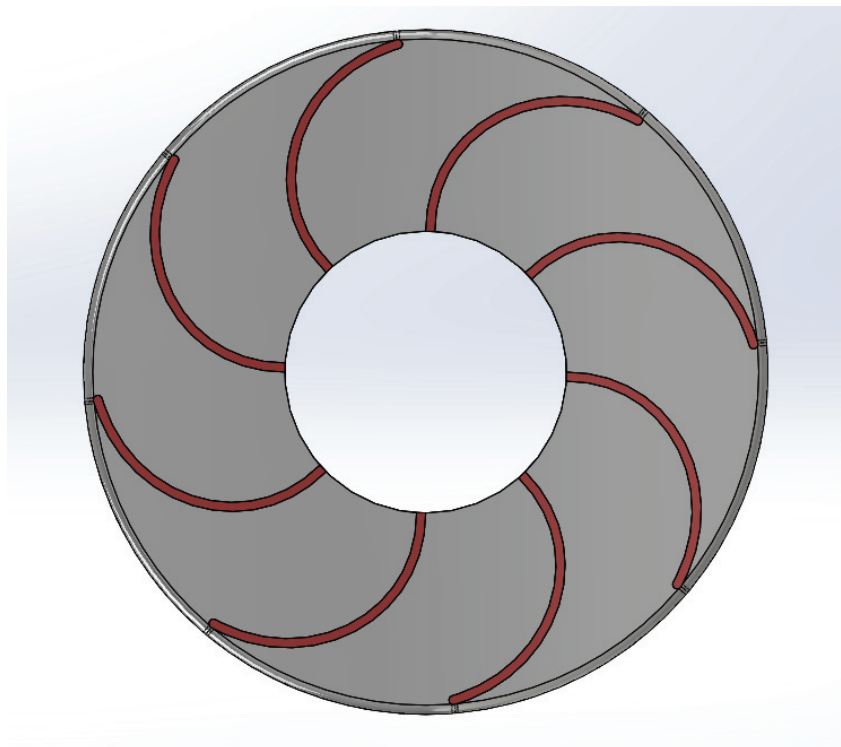
Figure 4.5 Top view of modified guide vane design

4.2 Simulation Results

The simulation of the modified model is done by applying the same conditions with the original model except the guide vane sections. In order to demonstrate that the modified design answers the purpose, velocity streamlines in guide vanes are shown in Figure 4.6.
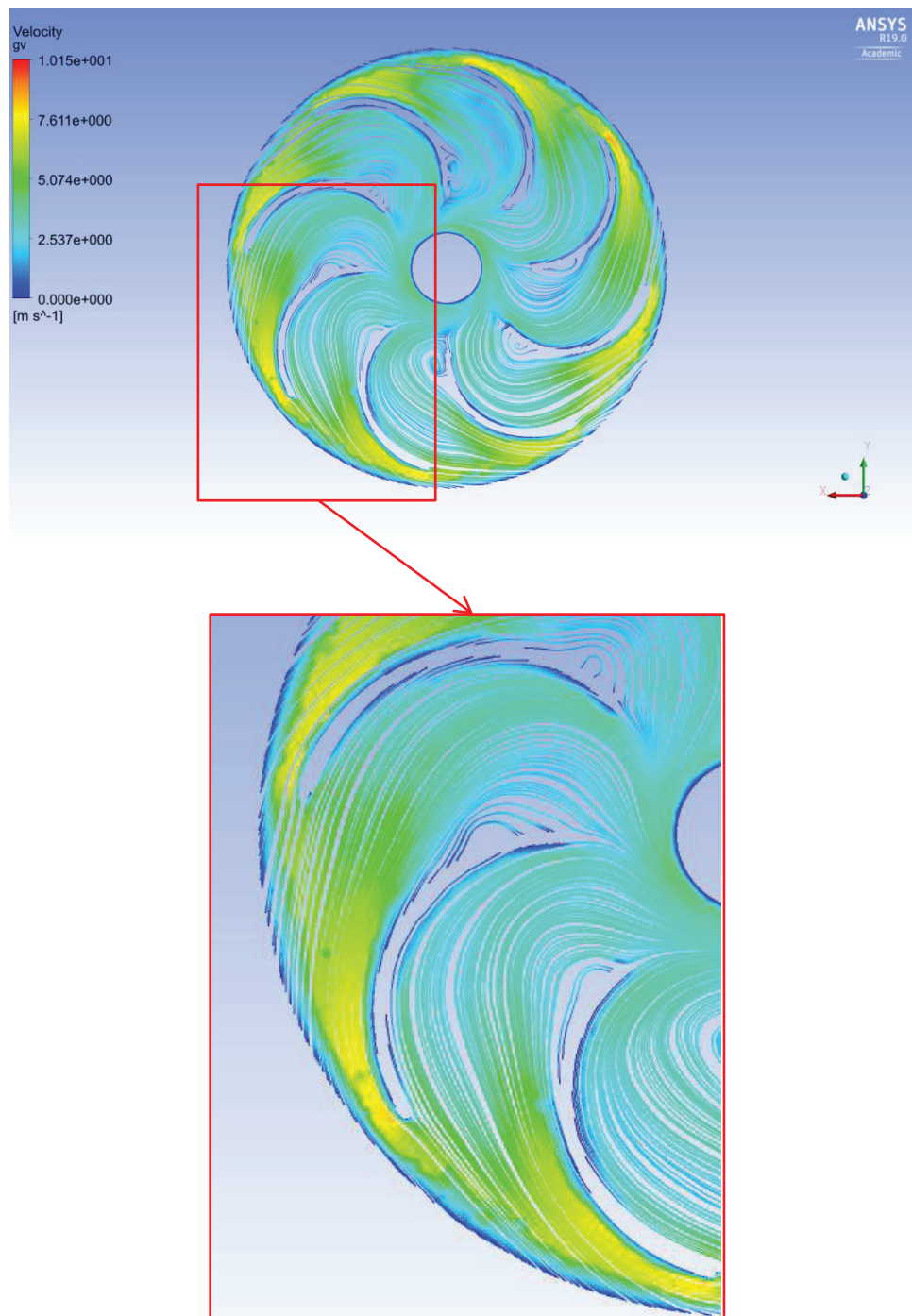
Figure 4.6 Velocity streamlines of modified design at guide vane section

It was expected that the flow in impeller section preserves the uniformity. In guide vane section, the inefficient swirls are decreased substantially. Distributing the bending of vane to entire geometry causes the flow separation to disappear at pressure sides.

The rotationary flow which comes out from impeller needs to travel between guide vanes in order to gain uniformity. As for the guide vane path is long, friction loss due to the wall shear increases. Otherwise, flow separations may not be eliminated. In order to investigate the effect of wrap angle, a set of CFD analysis has been done and the results were summerized in Table 4.2.

Table 4.2. Total pump head and overall guide vane efficiencies for different wrap angles

| Wrap Angle (°)	Total Head (m)	Guide Vane Efficiency	Loss Coefficient
30	24.1	0.89	0.59
40	24.7	0.90	0.46
50	23.6	0.91	0.45
60	23.1	0.91	0.43
90	20.7	0.87	0.47

It is seen that best the efficiencies are seen between 50 to 60 degrees of wrap angles with a little loss in head and the loss coefficients are close to each other except 30 degrees of wrap angle.

Nevertheless, it is seen from the data in Table 4.2, changes in wrap angle does not create big differences on guide vane efficiency as much as the pump head. It can be said that the small travel length differences of flow between vanes does not affect the tangential energy much which generate the inefficiency in guide vanes.

As it is seen in Figure 4.7, even though small velocity drops occur at the trailing edges of guide vanes for smaller wrap angles, the flow maintains its uniformity in the channels. No flow recirculations observed in return channels for any degrees of wrap angles. This indicates that forming a smooth curved vane is the main factor in order to eliminate the recirculations in channels.
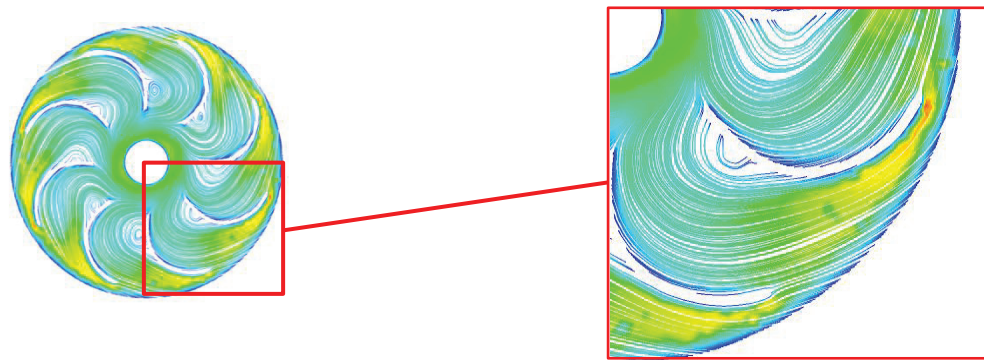
(a)
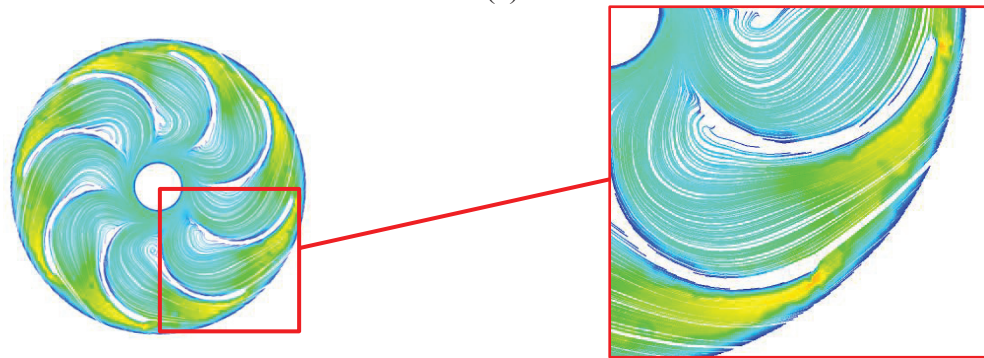
(b)
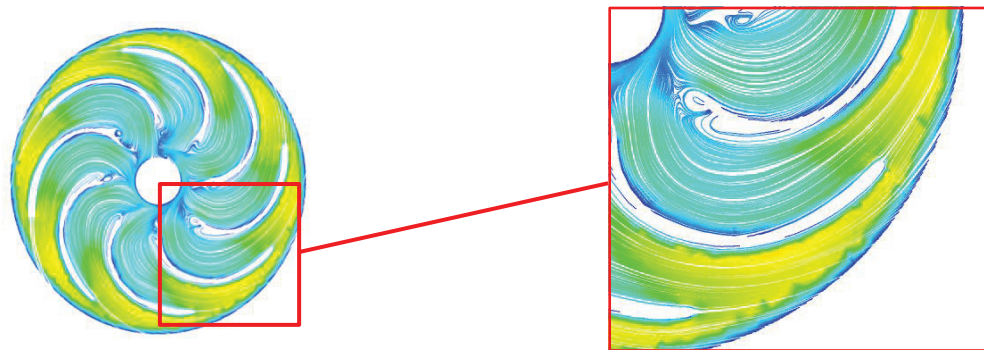
(c)
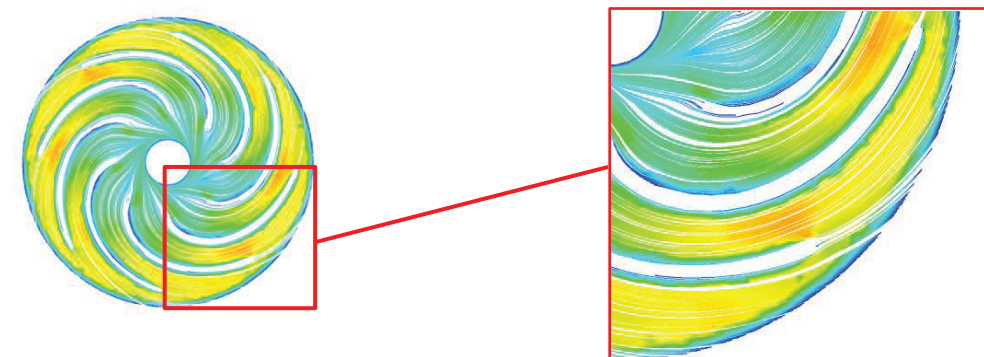
(d)

Figure 4.7 Velocity streamlines in guide vanes for different wrap angles (a) 30 degrees,(b) 40 degrees, (c) 60 degrees, (d) 90 degrees.

It is determined that the wrap angle of modified design is chosen as 40 degrees, since the key parameters of this study is the total head and the area blocking swirls. The performance parameters of modified design is given in Table 4.3.

Table 4.3 Performance parameters of modified design

Total head (m)	24.7
Pump efficiency	0.74
Loss coefficient	0.46

In addition to these, in order to verify that simulations are reliable, eight points are chosen on different streamlines between two blades and flow angles are read. The distance between blades is nondimensionalized and the flow angles with slip are demonstrated in Figure 4.8. According to Stodola's formula in Equation A.5, the calculated slip factor is 0.66 and this makes the flow angle 16.6 degrees.
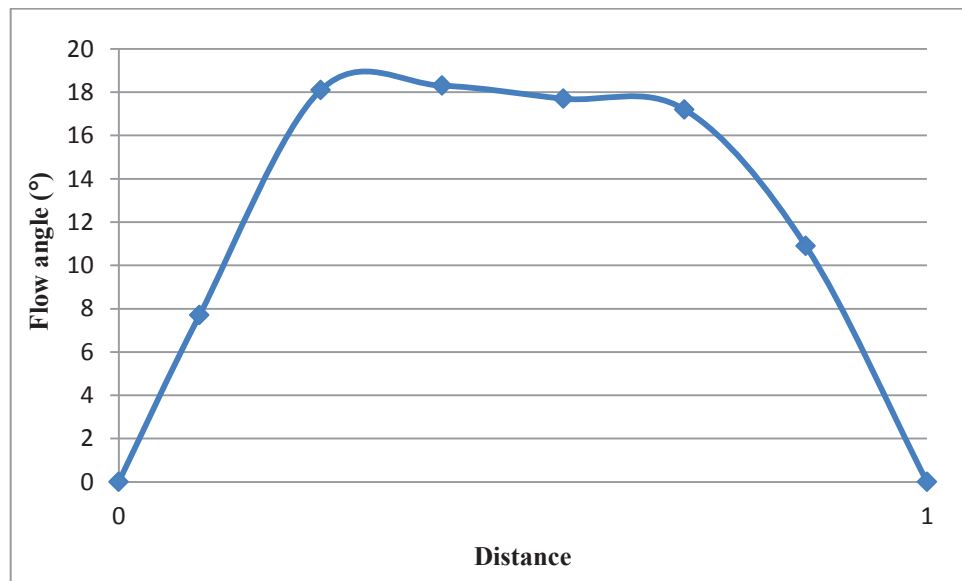
Figure 4.8 Flow angles between two impeller blades

At the points closer to the blades, flow angle is smaller due to the no slip condition. The flow angle is approximately 18 degrees around the mean streamline and it can be said that, this study can predict the flow angle with a deviation of 2 degrees in the basis of Stodola's approach.

As a comparison, total head and hydraulic efficiency graphs are given in Figure 4.9 and Figure 4.10.
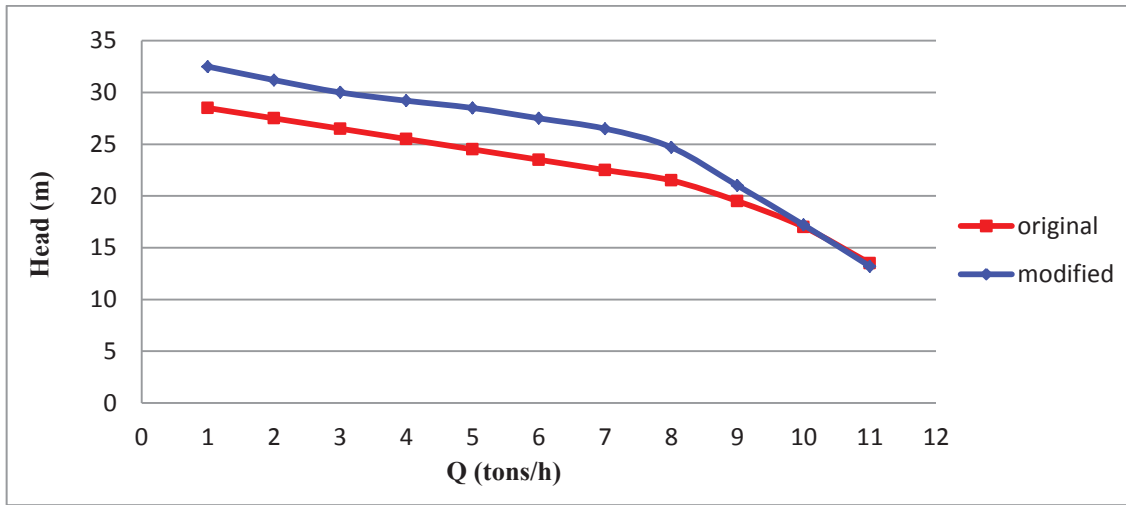
Figure 4.9 Head-capacity curves of original and modified design
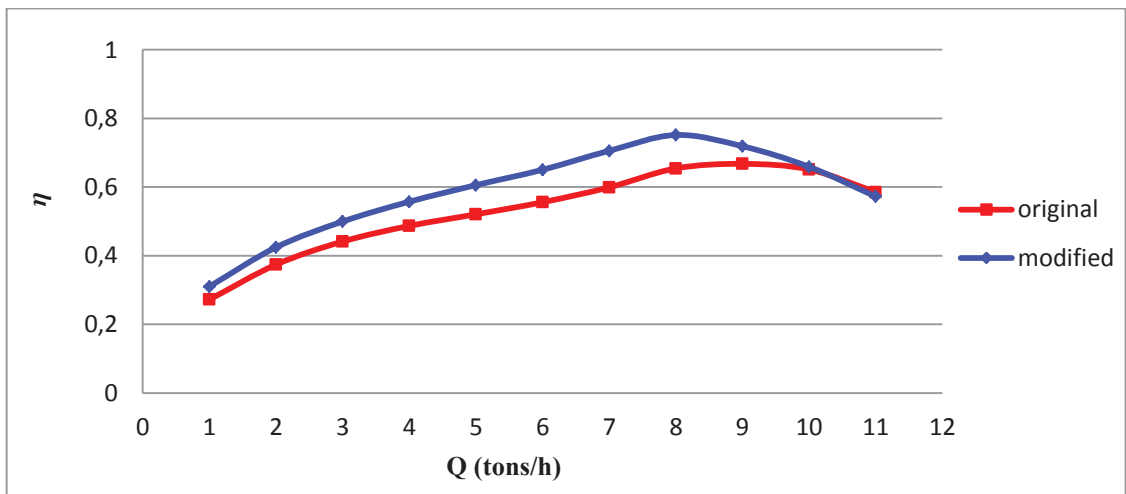
Figure 4.10 Efficiency-capacity curves of original and modified design

There is a visible head and efficiency difference between two designs until 9 tons/h of capacity. The best efficient point of this multistage pump is 8 tons/h and it is shown that the geometric modifications of guide vanes work correctly. The increase in total head and efficiency values can be explained by eliminating the deficiencies in guide vane section and it is demonstrated in Figure 4.11.
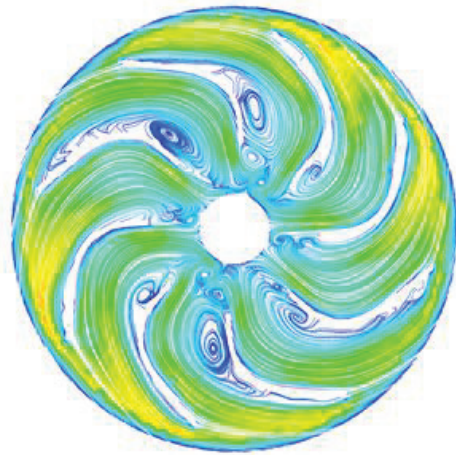
Original Guide Vane   Modified Design ($\theta = 40°$)

Figure 4.11 Velocity streamlines in guide vane sections of original and modified
design

CHAPTER 5

CONCLUSIONS

The objective of this thesis is to simulate a multistage submersible pump flow and reduce observed inefficiencies.

Simulation results indicated that there are recirculation regions in the flow passages of stationary parts which reduce the efficiency of the pump. It is considered that these recirculations are arisen from return channel blade geometry and several modifications were made to remove undesirable flow behaviour.

It was expected that enterance shocks occur when the flow travels through stages in vaned areas. Therefore, blade angles were adjusted based on the flow angle at impeller exit to minimize losses. Additionally, when the flow with high kinetic energy encounters a sharp turn, flow separations are shown up. Blade geometry was designed in the manner that there should not be any rapid changes in blade curvature, so as to prevent recirculation occurance.

Besides, several simulations were done with different wrap angles in order to see the relation between flow uniformity and travelled path between blades. As a result, an optimized wrap angle which is 40° is used on the basis of separation and frictional losses.

All these modifications considered, pump head at best efficiency point increased 14%, pump efficiency increased 12%, and loss coefficient decreased 50% for five stages of the pump.

In conclusion, the stationary parts of turbomachinery are seen inconsiderable in literature and industry because of not generating work. However, it is needed that loss recovery has to be paid attention and studied as much as generation. This study and future works aim at recovering the inefficiencies and improving the performance of turbomachineries.

APPENDIX A

CALCULATIONS

Operating conditions and design constraints which are provided by manufacturer are given as follows;

Table A.1 Conditions of original pump

H (m)	4,5	β_2 (°)	28
Q (m³/s)	0,0022	D_1 (m)	0,034
n (rpm)	2900	D_2 (m)	0,073
z	6	b_1 (m)	0,008
β_1 (°)	17	b_2 (m)	0,006

The velocity components at the impeller exit are calculated in order to specify the design parameters. The peripheral velocity at the outlet is;

$$u_2 = (\omega_2) * (D_2/2) = (2900 * \frac{2\pi}{60}) * (0,073/2) = 11,08 \text{ m/s} \qquad (A.1)$$

and the meridional velocity is calculated by using the flow rate;

$$V_{r_2} = \frac{Q}{2\pi r_2 b_2} = \frac{0,0022}{2 * \pi * \left(\frac{0,073}{2}\right) * 0,006} = 1,6 \text{ m/s} \qquad (A.2)$$

Tangential component of the absolute discharge velocity is;

$$V_{t_2} = u_2 - V_{r_2}(\cot\beta_2) = 8,07 \text{ m/s} \qquad (A.3)$$

The specific speed is calculated for one stage of the pump;

$$N_s = 51 * N_{s_m} = 51 * \frac{n * \sqrt{Q}}{H^{0,75}} = 51 * \frac{2900 * \sqrt{0,0022}}{4,48^{0,75}} \approx 2300 \qquad (A.4)$$

It is expressed in Pump Handbook that, design parameters are specified as $\frac{Vr2}{u2}$ and β_2, based on the commonly used values in industry. Figure A.1 shows the design ranges of mentioned parameters with respect to the specific speed values. It is recommended to take these ranges into consideration in order not to encounter manufacturing difficulties.

For this study, design parameters are calculated and ensured that they are in the desired range. $\frac{Vr2}{u2}$ and β_2 are marked in Figure A.1a and A.1b respectively where $\frac{Vr2}{u2}$ is 0,144 and β_2 is 28.

(a)   (b)
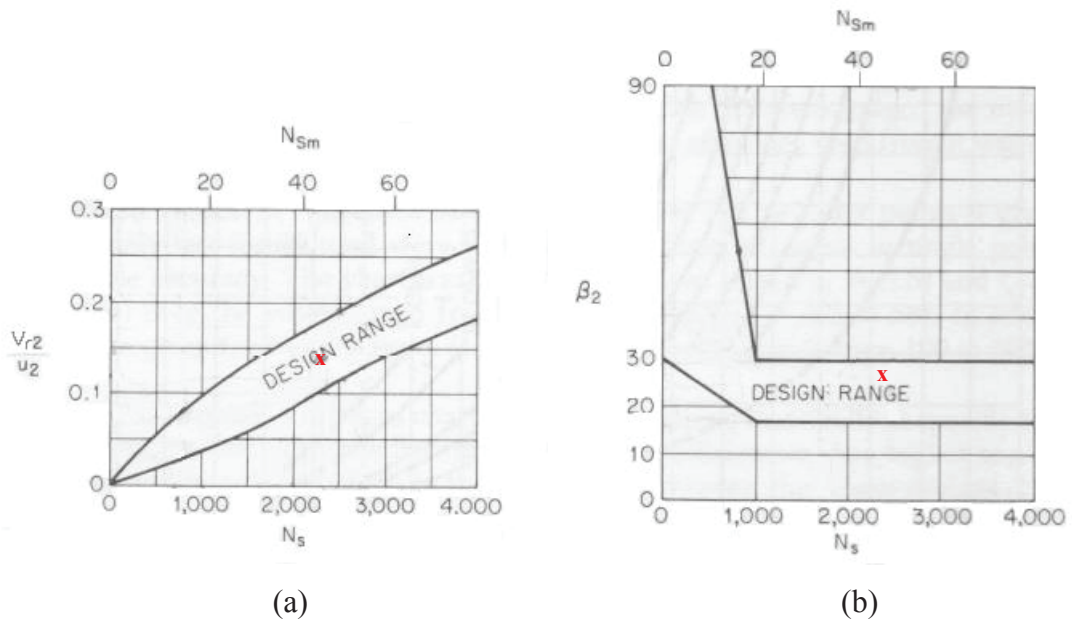
Figure A.1 Design ranges of parameters (Source: Karassik, et al. 1986), (a) $\frac{Vr2}{u2}$ versus specific speed, (b) β_2 versus specific speed

Another design parameter is the vane number of impeller, z which is needed to calculate the slip factor. Slip factor is an important measure to determine flow angle at the exit of the impeller. It is used to describe the deviation between the blade angle and flow angle. In order to determine the exact value of slip, experiments and detailed measurements should be obtained. In this study, Stodola's equation is used to predict the slip factor due to the comformability to investigated case.

$$\sigma = 1 - \frac{\pi}{z}\frac{sin\beta2}{\left(1-\frac{Vr2}{u2}\,cot\beta2\right)} = 0,66 \qquad (A.5)$$

REFERENCES

Abbas, Mohammed K., Ali Z. Asker, and Samir D. Ali. "Computation of hydrodynamic characteristics of water flow in electrical submersible pump." *Diyala Journal of Engineering Sciences, 5*, 2012: 37-51.

Aghaei tog, R., A. M. Tousi, and A. Tourani. "Comparison of turbulence methods in CFD analysis of compressible flows in radial turbomachines." *Aircraft Engineering and Aerospace Technology vol. 80*, 2008: 657-665.

Akaike, S., and T. Toyokura. "Flow in interstage return bend of centrifugal turbomachinery." *6th Conference on Fluid Machinery.* Budapest, 1979. 11-20.

ANSYS Inc. *ANSYS Fluent Theory Guide Release 15.0.* Canonsburg, PA: ANSYS, Inc., 2013.

Arutunoff, Armais. Electrically driven pump. US Patent 1,610,726. 14 December 1926.

Atkins, Tony, and Marcel Escudier. *A dictionary of Mechanical Engineering.* Oxford University Press, 2013.

Aungier, R.H. *Centrifugal Compressors: A Strategy for Aerodynamic Design and Analysis.* New York: ASME, 2000.

Bhaskaran, Rajesh, and Lance Collins. *Introduction to CFD basics.* Cornell University-Sibley School of Mechanical and Aerospace Engineering, 2002.

Blazek, J. *Computational Fluid Dynamics: Principles and Applications.* Oxford: Elsevier, 2001.

Bowade, Ashish, and Charu Parashar. "A Review of different blade design methods for radial blade centrifugal pumps." *International Journal of Scientific Engineering and Research (IJSER), 3*, 2015: 24-27.

Britannica, The Editors of Encyclopaedia. «Archimedes screw.» *Encyclopædia Britannica.* 7 March 2014. https://www.britannica.com/technology/Archimedes-screw (accessed December 21, 2018).

Campbeel, Dan, Noah Brown, and John Cox. "Centrifugal Pumps." *Colorado State University.* n.d. https://www.engr.colostate.edu/~pierre/ce_old/classes/CIVE%20401/projects%202015/Centrifugal%20Pumps%20.pdf (accessed January 18, 2019).

Chaurette, Jacques. *Centrifugal pump specific speed primer.* Montreal: Fluide Design Inc., 2003.

Collin, William. *Collins Dictionary of English Language.* London: William Collins Sons & Co. Ltd, 1984.

Cumpsty, Nick. *Compressor Aerodynamics.* Krieger Publishing Company, 2004.

Damor, Jekim J., Dilip S. Patel, Kamlesh H. Thakkar, ve Pragnesh K. Brahmbhatt. «Experimental and CFD analysis of centrifugal pump impeller - A case study.» *International Journal of Engineering Research & Technology, vol.2*, 2013.

Denton, John D. «Some limitations of turbomachinery CFD.» *Proceedings of ASME Turbo Expo 2010: Power for Land, Sea and Air*. Cambridge: ASME, 2010.

Elsey, Jim. *10 ways to improve your impeller*. 10 April 2017. https://www.pumpsandsystems.com/pumps/april-2017-10-ways-improve-your-impeller (accessed January 22, 2019).

Encyclopedia Britannica. *Archimedes screw*. 7 March 2014.

ESPpump.com. *ESPpump.com*. n.d. http://esppump.com/ (accessed 01 16, 2019).

Feng, Jianjun, Xingqi Luo, Guojun Zhu, ve Guangkuan Wu. «Investigation on disk friction loss and leakage effect on performance in a Francis model turbine.» *Advances in Mechanical Engineering 9*, 2017: 1-10.

Girdhar, Paresh, and Octo Moniz. *Practical Centrifugal Pump*. Oxford: Elsevier, 2004.

Harvey, Shane. «Centrifugal compressors in ethylene plants.» *AIChE*. February 2017. https://www.aiche.org/resources/publications/cep/2017/february/centrifugal-compressors-ethylene-plants (accessed March 28, 2019).

Hexa Research. *Electrical submersible pump (ESP) market analysis, market size, application analysis, regional outlook, competitive strategies and forecasts 2016 to 2024*. Hexa Research, November 2017.

Hildebrandt, A. «Aerodynamic optimisation of a centrifugal compressor return channel and U-turn with genetic algorithms.» *ASME Turbo Expo 2011*. Vancouver, 2011.

Hollund, Bernt Stale. *Artificial lift - Electrical submerged pumpi best practice and future demands within subsea applications*. Stavanger: University of Stavanger, 2010.

Hunt, J.C.R. «Lewis Fry Richardson and his contributions to mathematics, meteorology and models of conflict.» *Annual Review of Fluid Mechanics, 30*, 1998.

Hydra-Tech. *Different impeller types*. 13 April 2016. https://hydra-tech.com/9-different-impeller-types/ (accessed January 22, 2019).

Indiamart. *Open impeller*. n.d. (accessed January 22, 2019).

Jameson, Antony. «Computational fluid dynamics past, present and future.» *AMS Seminar*. 2012.

Japikse, David, William D. Marscher, and Raymond D. Furst. *Centrifugal Pump Design and Performance*. Vermont: Concepts ETI, 1997.

Jones, D. D., and D. H. Vanderholm. *Pumping Animal Wastes*. Indiana: Purdue University, n.d.

Karassik, Igor J., William C. Krutzsch, Warren H. Fraser, ve Joseph P. Messina. *Pump Handbook*. McGraw-Hill, 1986.

Khalil, Essam E. «CFD History and Applications.» *CFD Letter, 4*, 2012: 43-46.

Kyparissis, Spyridon D., Eleni C. Douvi, Elias E. Panagiotopoulos, Dionissios P. Margaris, ve Andronikos E. Filios. «Parametric study performance of a centrifugal pump based on simple and double-arc blade design methods.» *3rd International Conference on Experiments*. Athens, 2009.

Lee, Junghyun, Mohammad Moshfeghi, Nahmkeon Hur, and In Sik Yoon. "Flow analysis in a return channel of a multi-stage centrifugal pump." *Journal of Mechanical Science and Technology*, 2016: 3993-4000.

Li, Yaojun, and Fujun Wang. "Numerical investigation of performance of an axial-flow pump with inducer." *Journal of Hydrodynamics, 19*, 2007: 705-711.

Mc Nally Institute. *Open vs. closed impellers*. 2 February 2018.

Menter, F. R. «Two-equation eddy viscosity turbulence models for engineering applications.» *American Institute of Aeronautics and Astronautics, AIAA Journal*, 1994: 1598-1605.

Methel, Cam-Tu Jeanne. *An experimental comparison of diffuser designs in a centrifugal compressor*. Indiana: Purdue University, 2016.

«Modeling flows in moving zones.» *ANSYS Fluent User's Guide Release 15.0*. November 2013. http://www.pmt.usp.br/ACADEMIC/martoran/NotasModelosGrad/ANSYS%20Fluent%20Users%20Guide.pdf (accessed March 18, 2019).

New Mexico Tech. *Advanced artificial lift methods*. 2015.

«Numerical investigations and performance experiments of a deep-well centrifugal pump with different diffusers.» tarih yok.

Oshinowo, Lanre, Zdzislaw Jaworski, Kate N. Dyster, Elizabeth Marshall, ve Alwin W Nienow. «Predicting the tangential velocity field in stirred tanks using the Multiple Reference Frames (MRF) model with validation by LDA measurements.» *10th European Conference on Mixing*. Delft: Elsevier, 2000. 281-288.

Oyelami, A.T., S.B. Adejuyigbe, M.A. Waheed, A.K. Ogunkoya, and D. Iliya. "Analysis of radial-flow impellers of different configurations." *The Pacific Journal of Science and Technology, 13*, 2012: 24-33.

Pinto, Runa Nivea, Asif Afzal, Loyan Winson D'Souza, Zahid Ansari, and Mohammer A.D. Samee. "Computational fluid dynamics in turbomachinery: A review of state of the art." *Archives of Computational Methods in Engineering*, 2016.

Rangarajan, Ajay Mandyam. *What is the difference between CFD and EFD?* 30 July 2013. https://www.quora.com/What-is-the-difference-between-CFD-Computational-Fluid-Dynamics-and-EFD-Experimental-Fluid-Dynamics (December 221, 2018 tarihinde erişilmiştir).

Robinson, Henry William. «Denis Papin (1647-1712).» *The Royal Society journal of the history of science, 5*, 1947.

Roclawski, H., A. Weiten , and D.-H. Hellmann. "Numerical investigation and optimization of a stator for a radial submersible pump stage with minimum stage diameter." *European Fluids Engineering Summer Meeting*. Miami: ASME, 2006.

Sadrehaghighi, Ideen. *Essentials of turbomachinery in CFD.* Annapolis: CFD Open Series, 2018.

Sankaran, Venkateswaran, and Charles Merkle. *Comparison of pressure-based and density-based methods for low mach number CFD computations.* Purdue University, n.d.

Schlichting, Hermann , and Klaus Gersten. *Boundary-Layer Theory.* Berlin: Springer-Verlag, 2017.

Shi, Wei-dong, Wei-gang Lu, Hong-liang Wang, and Qi-feng Li. "Research on the theory and design methods of the new type submersible pump for deep well." *Fluids Engineering Division Summer Meeting.* Colorado: ASME, 2009.

Sjodin, Bjorn. *What's the difference between FEM, FDM, and FVM?* 4 April 2016. http://machinedesign.com/fea-and-simulation/what-s-difference-between-fem-fdm-and-fvm (accessed January 8, 2019).

Stel, H., T. Sirino, R.E.M. Morales, S. Chiva, ve F.J. Ponce. «Numerical investigation of the flow in a multistage electric submersible pump.» *Journal of Petroleum Science and Engineering 136*, 2015: 41-54.

Stepanoff, Alexey Joakim. *Centrifugal and Axial Flow Pumps.* Florida: Krieger Publishing Company, 1957.

Takacs, Gabor. *Electrical Submersible Pump Manual.* Oxford: Elsevier, 2009.

Tamaki, Hideaki, Satoshi Oouchida, Masaru Unno, Ryuuta Tanaka, and Satoshi Yamaguchi. "Enhancement of centrifugal compressor operating range by use of inlet fins." *IHI Engineering Review, 49*, 2016: 44-55.

Tao, Ran, Ruofu Xiao, Wei Yang, ve Fujun Wang. «A comperative assesment of Spalart-Shur rotation/curvature correction in RANS simulations in a centrifugal pump impeller.» *Mathematical Problems in Engineering*, September 2014.

Turunen-Saaresti, Teemu. *Computational and experimental analysis of flow field in the diffusers of centrifugal compressors.* Lappeenranta University of Technology, 2004.

Versteeg, H. K., and W. Malalasekera. *An Introduction to Computational Fluid Dynamics.* Essex: Peasoned, 2007.

Wei, Qingshun, and Xihuan Sun. "Performance influence in submersible pump with different diffuser inlet widths." *Advances in Mechanical Engineering, 9*, 2017: 1-8.

Wendt, John F. *Computational Fluid Dynamics.* Springer-Verlag, 2009.

Wood, G. M., H. Welna, and R. P. Lamers. "Tip-clearance effects in centrifugal pumps." *Journal of Basic Engineering*, 1965: 932-939.

Yannopoulos, Stavros I., et al. «Evolution of water lifting devices (pumps) over the century worldwide.» *Water, 7*, 2015: 5031-5060.

Zhao, W. G., Y. B. Li, X. Y. Wang, J. P. Sun, ve G. X. Wu. «Research on the effect of wear-ring clearances to the performance of centrifugal pump.» *26th IAHR Symposium on Hydraulic Machinery and Systems .* IOP Publishing, 2012.

Zhou, Ling, and Weidong Shi. "Numerical investigations and performance experiments of a deep-well centrifugal pump with different diffusers." *Journal of Fluids Engineering, 134*, 2012.

Zhu, Jianjun, and Hong-Quan Zhang. "A review of experiments and modeling of gas-liquid flow in electrical submersible pumps." *Energies, 11, 180*, 2018.